© 2017. Published by The Company of Biologists Ltd | Development (2017) 144, 1735 doi:10.1242/dev.153130

CORRECTION

Correction: Prdm16 is crucial for progression of the multipolar phase during neural differentiation of the developing neocortex

Mayuko Inoue, Ryota Iwai, Hidenori Tabata, Daijiro Konno, Mariko Komabayashi-Suzuki, Chisato Watanabe, Hiroko Iwanari, Yasuhiro Mochizuki, Takao Hamakubo, Fumio Matsuzaki, Koh-ichi Nagata and Ken-ichi Mizutani

There was an error published in Development **144**, 385-399.

In the data availability section, the accession information for the microarray data was incomplete. The full information is as follows: Microarray data have been deposited at ArrayExpress under accession numbers E-MTAB-5438 and E-MTAB-5646.

The authors apologise to readers for this mistake.

© 2017. Published by The Company of Biologists Ltd | Development (2017) 144, 385-399 doi:10.1242/dev.136382

STEM CELLS AND REGENERATION

RESEARCH ARTICLE

Prdm16 is crucial for progression of the multipolar phase during neural differentiation of the developing neocortex

Mayuko Inoue[1,*], Ryota Iwai[1,*], Hidenori Tabata[2], Daijiro Konno[3], Mariko Komabayashi-Suzuki[1], Chisato Watanabe[1], Hiroko Iwanari[4], Yasuhiro Mochizuki[4], Takao Hamakubo[4], Fumio Matsuzaki[3], Koh-ichi Nagata[2] and Ken-ichi Mizutani[1,5,‡]

ABSTRACT

The precise control of neuronal migration and morphological changes during differentiation is essential for neocortical development. We hypothesized that the transition of progenitors through progressive stages of differentiation involves dynamic changes in levels of mitochondrial reactive oxygen species (mtROS), depending on cell requirements. We found that progenitors had higher levels of mtROS, but that these levels were significantly decreased with differentiation. The *Prdm16* gene was identified as a candidate modulator of mtROS using microarray analysis, and was specifically expressed by progenitors in the ventricular zone. However, *Prdm16* expression declined during the transition into NeuroD1-positive multipolar cells. Subsequently, repression of Prdm16 expression by NeuroD1 on the periphery of ventricular zone was crucial for appropriate progression of the multipolar phase and was required for normal cellular development. Furthermore, time-lapse imaging experiments revealed abnormal migration and morphological changes in Prdm16-overexpressing and -knockdown cells. Reporter assays and mtROS determinations demonstrated that PGC1α is a major downstream effector of Prdm16 and NeuroD1, and is required for regulation of the multipolar phase and characteristic modes of migration. Taken together, these data suggest that Prdm16 plays an important role in dynamic cellular redox changes in developing neocortex during neural differentiation.

KEY WORDS: Neocortical development, Neural differentiation, Neural stem cells, Multipolar phase, Prdm16, NeuroD1, Mouse

INTRODUCTION

During neocortical development, newborn neurons undergo multiphasic radial migration processes to reach their final position within the cortical plate (CP). During this process, postmitotic immature neurons originate from radial glial progenitors and remain in the ventricular zone (VZ) for more than 10 h (Tabata and Nakajima, 2003; Noctor et al., 2004; Tabata et al., 2009, 2012, 2013) prior to transforming into multipolar cells that move out of VZ towards the intermediate zone (IZ). These multipolar cells remain just above VZ, in the multipolar cell accumulation zone (MAZ), for ∼24 h, where they acquire a multipolar morphology and actively extend and retract dynamic processes (Tabata and Nakajima, 2003; Noctor et al., 2004; Tabata et al., 2009, 2012, 2013) in the multipolar phase (Fig. S1A). Subsequently, they transform from a multipolar to a bipolar morphology that is suitable for locomotion along the radial glial fibers before entering the subplate (SP) and CP (Rakic, 1972; Nadarajah et al., 2001). Recently, the importance of the multipolar migratory phase involved in mature cortical network assembly has received substantial attention (LoTurco and Bai, 2006; Torii et al., 2009; Costa and Hedin-Pereira, 2010; Yamagishi et al., 2011; Miyoshi and Fishell, 2012; Ohtaka-Maruyama et al., 2013; Inoue et al., 2014). The early postmitotic neuronal marker NeuroD1 is highly localized to MAZ (Tabata et al., 2009, 2012, 2013), and downregulation of NeuroD1 in the early multipolar phase enables cells to initiate Unc5D (a marker for late multipolar cells) expression, which facilitates their transition from the early to the late multipolar phase (Fig. S1A) and is thus crucial for their migration through the IZ (Yamagishi et al., 2011; Miyoshi and Fishell, 2012; Inoue et al., 2014). This dynamic expression change is required for the cells to transition out of the multipolar state and into the CP, although the precise genetic controls at this stage are not well understood.

Controlled delivery and use of oxygen are essential for maintaining the balance between energy generation and avoiding unwarranted oxidation. During oxidative phosphorylation, mitochondria use oxygen to generate ATP from organic fuel molecules, but in the process they also produce intracellular reactive oxygen species (ROS) (Shadel and Horvath, 2015). Although ROS have long been known for their damage-promoting detrimental effects, their roles as signaling molecules are now becoming better understood (Shadel and Horvath, 2015). In particular, mitochondrial ROS (mtROS) signaling has also been implicated in homeostatic processes, including cellular differentiation (Hamanaka and Chandel, 2010; Tormos et al., 2011; Hamanaka et al., 2013). A recent study demonstrated that multipotent neural progenitors maintain a high level of ROS (Le Belle et al., 2011). Furthermore, an analysis of gene expression profiles from embryonic stem cell-derived neurosphere (NS) culture revealed that neuronal differentiation is accompanied by upregulation of pathways related to mitochondrial DNA (mtDNA) contents, mtROS generation and hypoxia, thereby underlying the importance of oxygen sensing in the cellular processes related to neural differentiation (Moliner et al., 2008).

We hypothesized that the transition of progenitors through progressive multipolar migratory phases, which requires drastic morphological changes and characteristic migration modes, probably involves dynamic changes in mtROS, depending on the needs of the cell. In particular, we aimed to elucidate the role of

[1]Laboratory of Neural Differentiation, Graduate School of Brain Science, Doshisha University, Kyoto 6190225, Japan. [2]Department of Molecular Neurobiology, Institute for Developmental Research, Kasugai, Aichi 4800392, Japan. [3]Laboratory for Cell Asymmetry, Center for Developmental Biology, RIKEN Kobe Institute, 2-2-3 Minatojima-minamimachi, Chuo-ku, Kobe, Hyogo 650-0047, Japan. [4]Department of Quantitative Biology and Medicine, RCAST, The University of Tokyo, Tokyo 1538904, Japan. [5]PRESTO "Development and Function of Neural Networks", Japan Science and Technology Agency, Saitama 3320012, Japan.
*These authors contributed equally to this work

‡Author for correspondence (kmizutan@mail.doshisha.ac.jp)

K.M., 0000-0001-6007-1132

Received 14 February 2016; Accepted 6 December 2016

Development (2017) 144, 385-399 doi:10.1242/dev.136382

mtROS during neural differentiation and identify a candidate modulator of mtROS during neocortical development.

RESULTS

Cellular mtROS levels change with differentiation

To determine endogenous mtROS levels in neocortical cells, we performed fluorescence-activated cell sorting (FACS) using the mtROS-sensitive chemical probe MitoSox (Robinson et al., 2008). Specifically, we dissociated embryonic day 14.5 (E14.5) neocortical cells and performed FACS analyses using an anti-CD133 antibody (neural progenitor marker) conjugated to a fluorescent dye (Fig. 1A; Mizutani et al., 2007).

Neural progenitor cells maintained a high level of ROS, which is consistent with a previous study (Le Belle et al., 2011), and cellular MitoSox levels (mtROS levels) were positively correlated with CD133 expression. Therefore, we quantified changes in mtROS levels of neocortical cells at E10.5, E14.5 and E17.5 (Fig. 1A,B). Neocortical cells were clearly separated into cell populations with high (mtROS^{high}) and low levels of mtROS (mtROS^{low}). In addition, relative proportions of mtROS^{high} and mtROS^{low} cells changed during neocortical development (Fig. 1B), and the mtROS^{high} Neuro2a cell populations decreased significantly after treatment with retinoic acid (RA; Fig. 1C). Conversely, other ROS species-sensitive dyes, such as DCFDA for total ROS (Fig. 1D), DAF for peroxides (Fig. 1E) and HPF for hydroxyl radical (data not shown), did not show marked changes during neural differentiation.

To examine changes in mtDNA contents (Puente et al., 2014) during neural differentiation (Fig. 1F), we collected GFP^{+} cells using FACS at 24, 36 and 48 h after *in utero* electroporation (IUE) (Mizutani et al., 2005, 2007; Inoue et al., 2014, 2015; Yamanishi et al., 2015) of CAG-EGFP plasmid at E14.5. Subsequent comparisons with mtDNA mRNA levels using quantitative polymerase chain reaction (qPCR) (Fig. 1F), showed that mtDNA copy numbers decrease linearly during differentiation. These results suggest that neural progenitor cells have higher mtROS levels, which decrease significantly with differentiation.

Identification of a candidate modulator of mtROS

In further transient transfection experiments in neocortical primary cultures, we used a plasmid containing neural basic helix-loop-helix Hes1, neurogenin 2 (Ngn2) and NeuroD1 promoter regions fused to the luciferase reporter gene. Following culture in the presence of a mtROS inhibitor of lipoic acid (LA), which is an essential co-enzyme in mitochondrial multienzyme complexes, Hes1 promoter activity was significantly suppressed, whereas both Ngn2 and NeuroD1 promoter activities were significantly increased (Fig. 2A). Moreover, expression profiling in qPCR, gain-of-function analyses of mt-target catalase (mt-Cat; Schriner et al., 2005) in primary cultures showed that overexpression of mt-Cat increased the expression of pro-neural genes such as Ngn2 and NeuroD1, and decreased Hes1 expression levels (Fig. 2B). Therefore, we hypothesized that neural differentiation (Fig. S1A) occurs in response to dramatic decreases in cellular mtROS levels. To quantify changes in cellular mtROS levels during differentiation, we used FACS to separate E14.5 neocortical cells into mtROS^{high} and mtROS^{low} cell populations (Fig. S1B) and compared expression profiles using qPCR (Fig. 2C). In these experiments, mtROS^{high} cells expressed significantly higher levels of the stem/progenitor marker Pax6, whereas mtROS^{low} cells expressed significantly higher levels of the early multipolar cell marker NeuroD1 (Seo et al., 2007; Tabata et al., 2009, 2012, 2013; Miyoshi and Fishell, 2012; Inoue et al., 2014) and the late multipolar cell marker Unc5D (Miyoshi and Fishell, 2012; Inoue et al., 2014). In addition, we compared expression profiles after separating three gates (Fig. S1C) and found that gated populations were distinguished by differing markers as follows: Pax6 (gate 1), NeuroD1 (gate 2) and Unc5D (gate 3). Hence, mtROS levels are markedly altered during the transition of progenitor cells to postmitotic multipolar cells.

During the transition of progenitors to postmitotic cells, remarkable changes in mtROS levels between mtROS^{high} and mtROS^{low} cells may reflect regulation of genes that are associated with antioxidative and oxidative activities, respectively. Accordingly, stem cells have unique mechanisms for coping with accumulated ROS, involving increased antioxidant defenses and unique redox-dependent effects on growth and differentiation (Csete et al., 2001; Saretzki et al., 2004; Piccoli et al., 2005). Thus, in further studies, we used FACS to separate E14.5 neocortical cells into mtROS^{high} and mtROS^{low} cell populations, and compared their expression profiles. However, comparisons of mtROS^{high} and mtROS^{low} cells using DNA microarrays revealed no changes in the expression of genes that are known to regulate redox homeostasis, including superoxide dismutase genes (*Sod1*, *Sod2*), *Cat*, *FoxO* genes, *APE-Ref-1* (*Apex1*), *Nrf2* (*Gabpa*), *Atm*, *Ahsa1* and *Trp53* (Table 1), but showed a twofold increase in the expression of PR (PRD1-BF-1-RIZ1 homologous) domain-containing protein 16 (*Prdm16*).

Prdm16 is a transcription factor that regulates energy balance and contributes to brown fat development (Seale et al., 2008; Kajimura et al., 2010; Trajkovski et al., 2012). A recent study showed that Prdm16 is preferentially expressed by adult neural stem cells and is required for their maintenance, partly by modulating oxidative stress (Chuikov et al., 2010). Therefore, we transfected Neuro2a cells with psh-Prdm16 plasmids and determined mtROS levels after 24, 36 and 48 h of culture. Subsequently, mtROS levels were significantly decreased in Prdm16 loss-of-function cells (Fig. 2D). In addition, Prdm16 loss-of-function vector significantly decreased mtDNA contents (Fig. 2E).

Taken together, these results suggest that the dynamic changes in mtROS levels during differentiation are closely correlated with stepwise regulation of the cell state, and that these levels change markedly when progenitor cells transition into postmitotic multipolar cells. In addition, Prdm16 was identified as a possible candidate for mtROS modulation in the developing neocortex.

Prdm16 is specifically expressed in the VZ

Based on the above results, we tested whether Prdm16 is required for neocortical development as an attenuator of cellular mtROS levels during neural differentiation. Using antibody against Prdm16 (Fig. S1D), we demonstrated strong expression in the developing neocortex, especially from E12.5 to E16.5 (Fig. S2A). In addition, Prdm16 was expressed in progenitor cells, and was upregulated in the VZ (Fig. 3A) and in areas that were positive for Pax6 (Fig. S2B). However, Prdm16 was downregulated around the MAZ, the lower portion of the IZ (Fig. 3B) and in areas that were positive for NeuroD1 (Tabata et al., 2009, 2012, 2013; Miyoshi and Fishell, 2012; Inoue et al., 2014). Hence, Prdm16 expression was predominantly downregulated in postmitotic cells located outside the VZ. Moreover, expression patterns for Prdm16 and NeuroD1 were complementary (Fig. 3B‴,C‴), as corroborated in immunostaining experiments that showed strong Prdm16 expression and negative positivity for NeuroD1 in primary cultures. Conversely, cells that were strongly positive for NeuroD1 were negative for Prdm16 (Fig. 3D‴,E). In further experiments, GFP-positive cells were identified in the MAZ after 36 h of IUE (Tabata et al., 2009); these GFP-positive cells separated three areas positioned below the SP into the VZ, the MAZ and the IZ (Fig. S2C and see microscopy and imaging analysis in the supplementary Materials and Methods). Prdm16 expression was

Development (2017) 144, 385-399 doi:10.1242/dev.136382

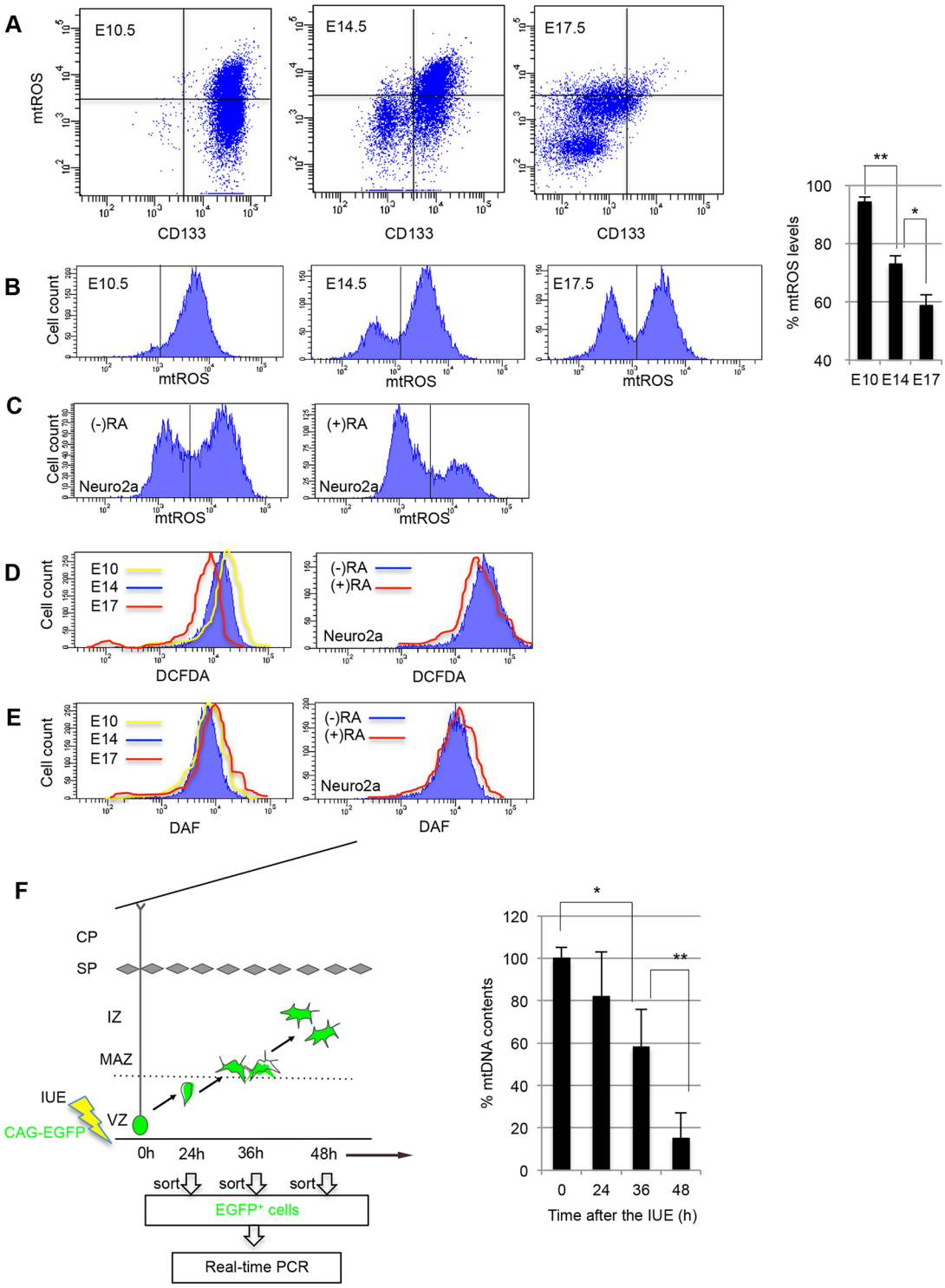

Fig. 1. Cellular mtROS levels significantly decrease with differentiation. (A) Relative mitochondrial reactive oxygen species (mtROS) levels were measured in flow cytometry experiments using the ROS-sensitive dye MitoSox in embryonic day (E) 10.5, E14.5 and E17.5 neocortical dissociated cells that were stained with the neural stem cell marker CD133-APC. (B) mtROS levels were detected using MitoSox in E10.5, E14.5 and E17.5 dissociated neocortical cells. Quantitative analysis of endogenous mtROS levels at each embryonic stage; **P*<0.01, ***P*<0.001; *n*=10 independent experiments. (C) mtROS levels in Neuro2a cells cultured with or without retinoic acid (RA). Relative endogenous ROS levels in neocortical cells were also measured using the ROS-sensitive dyes (D) DCFDA and (E) DAF. (F) FACS analysis was performed to sort GFP$^+$ cells 24, 36 and 48 h after *in utero* electroporation (IUE) of CAG-EGFP plasmid at E14.5. mtDNA levels were compared using qPCR; **P*<0.01, ***P*<0.001; *n*=3 independent experiments.

compared with GFP expression (Fig. 3F). Prdm16 expression gradually decreased with the transition of progenitors through the progressive stages of differentiation from the VZ to the IZ. In addition, the developing cortex from the ventricle face to the lower region of the IZ was divided into four bins (Fig. 3B′″), and numbers of cells that were strongly (++) or weakly (+) positive for Prdm16 or

Development (2017) 144, 385-399 doi:10.1242/dev.136382

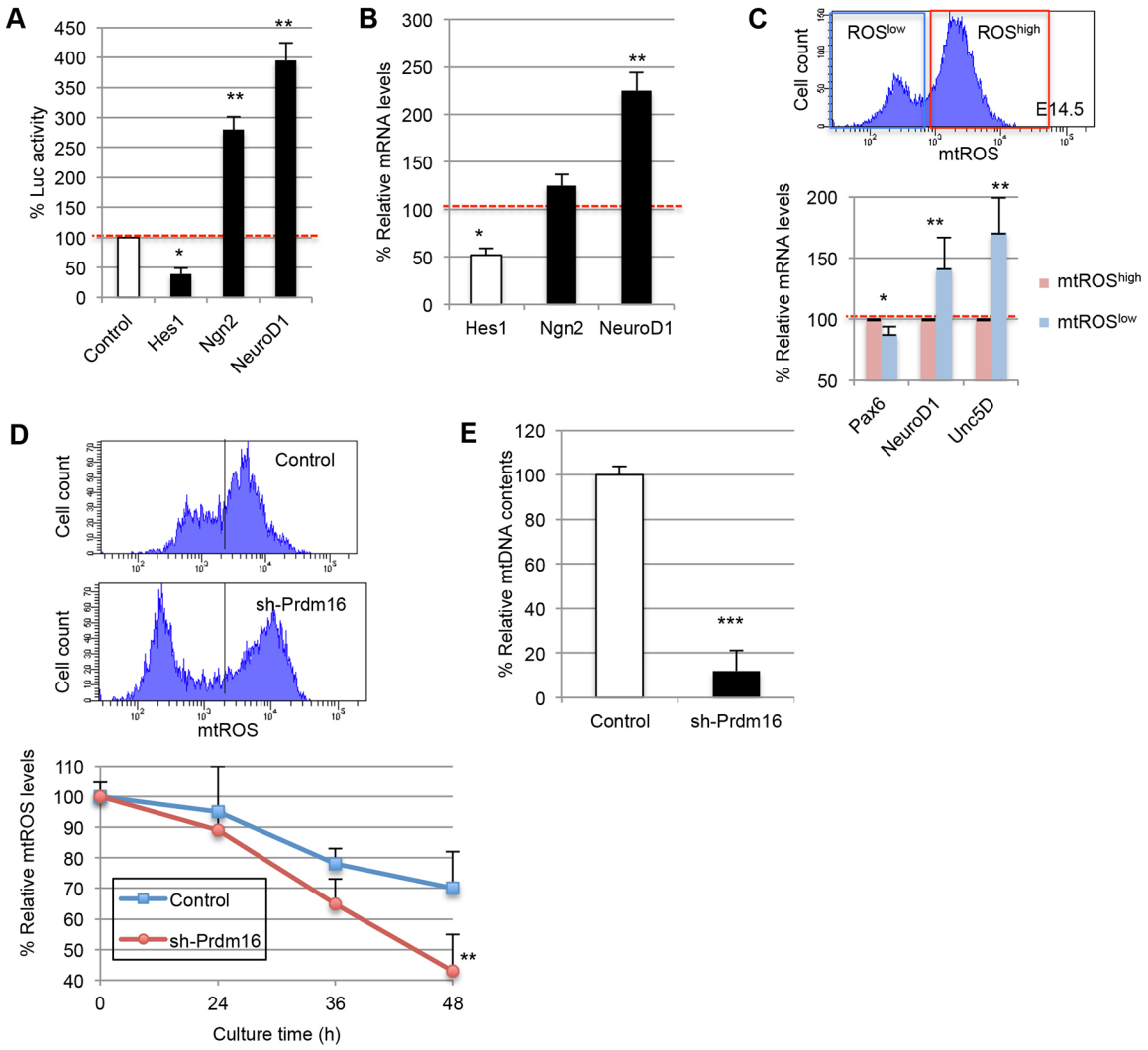

Fig. 2. Dynamic changes in mtROS levels are closely correlated with differentiation levels. (A) Reporter constructs were designed to express firefly luciferase in response to Hes1, Ngn2 and NeuroD1, and were transfected into primary cultures with or without mtROS inhibitors; *P<0.01, **P<0.001; n=5 independent experiments. (B) qPCR analysis of transcriptional factors in primary cultures after co-transfection of CAG-EGFP and mt-Cat overexpression; *P<0.01, **P<0.001; n=5 independent experiments. (C) To determine cell characteristics, populations with different mtROS levels were isolated at E14.5, and expression profiling for marker genes was performed; *P<0.01, **P<0.001; n=5 independent experiments from different littermates. (D) FACS plot of mtROS in neocortical primary cultures transfected with control or sh-Prdm16; mtROS levels were quantified using flow cytometry after staining with MitoSox in culture for various times; **P<0.001; n=7 independent experiments. (E) Relative mtDNA contents were determined in neocortical primary cultures transfected with control of sh-Prdm16; ***P<0.0001; n=3 independent experiments.

NeuroD1 were quantified and compared (Fig. 3G). In these analyses, cells in the VZ expressed only Prdm16, whereas those in the MAZ expressed both NeuroD1 and Prdm16; those in the lower part of the IZ expressed only NeuroD1, indicating that neural progenitor cells specifically express Prdm16. However, Prdm16 expression declined with the transition into NeuroD1-positive multipolar cells from the MAZ to the lower region of the IZ.

Prdm16 regulates the development of postmitotic multipolar cells

In accordance with *in vitro* gain- and loss-of-function analyses of Prdm16, NS frequency and EdU labeling assays (Fig. 4A,B) showed decreased percentages of proliferating cells, suggesting that precise expression of Prdm16 is crucial for the transition of progenitors into postmitotic cells.

Subsequently, we performed Prdm16 gain- and loss-of-function experiments to test *in vivo* function within the developing neocortex. Three days after IUE at E12.5 (Fig. 4C and Fig. S3B), most Prdm16 gain-of-function cells possessed multipolar morphologies within the VZ and the IZ. By contrast, electroporated control vector cells were broadly distributed within the VZ, the IZ and the CP, and many differentiated neurons were observed. Statistical analyses revealed the significant effects of Prdm16 gain of function in the lower IZ (Bin 2; P<0.001), and the CP (Bin 4 and 5; P<0.01) but not in the VZ (Bin 1) or the upper IZ (Bin 3, Fig. 4D). By contrast, the majority of Prdm16 loss-of-function cells remained within the upper IZ (Fig. 4C and Fig. S3A) and had aberrant shapes, leading to inhibition of CP invasion (Fig. S3C). In further experiments, we labeled multipolar cells with a Cre-loxP clonal expression plasmid system comprising pCAG-FloxP-EGFP-N1 and pCAG-Cre (Shitamukai et al., 2011), and monitored morphological differences using IUE (Fig. 4E, Movies 1-3). The ensuing data showed that upregulation and downregulation of Prdm16 led to increased or decreased numbers of

Development (2017) 144, 385-399 doi:10.1242/dev.136382

Table 1. Microarray analysis of ROS^{high} versus ROS^{low} cells

Gene symbol	Fold change	Gene name
Sod1	1.121	Superoxide dismutase 1, soluble
Sod2	0.941	Superoxide dismutase 2, mitochondrial
Sod3	1.122	Superoxide dismutase 3, extracellular
Gpx1	1.432	Glutathione peroxidase 1
Gpx2	1.098	Glutathione peroxidase 2
Gpx3	0.898	Glutathione peroxidase 3
Gpx4	1.421	Glutathione peroxidase 4
Gpx5	1.122	Glutathione peroxidase 5
Foxo1	1.002	Forkhead box O1
Foxo3	1.221	Forkhead box O3
Foxo4	1.329	Forkhead box O4
Foxo6	1.221	Forkhead box O6
Nrf1	1.212	Nuclear respiratory factor 1
Atm	0.972	Ataxia telangiectasia mutated homolog
Prdm16	2.389	PR domain containing 16
Jnk1 (*Mapk8*)	0.718	Mitogen-activated protein kinase 8
Hif1a	1.101	Hypoxia inducible factor 1, alpha subunit
Hgf	1.341	Hepatocyte growth factor

Gene expression profiles of mtROS^{high} and mtROS^{low} cells from E14.5 neocortical tissues were compared using microarray (two independent samples) analyses. Representative genes that were correlated with ROS homeostasis are listed.

multipolar cells in the IZ, respectively (Fig. 4F), suggesting that Prdm16 is an important factor for the precise regulation of the transition from progenitors to postmitotic multipolar cells.

Prdm16 function depends on the zinc finger at its N-terminal domain (nZF) and directs normal NeuroD1 expression

Similar to other studies, we showed that NeuroD1 is highly localized to early multipolar cells immediately after the cells transition to a multipolar morphology in the MAZ or the lower IZ (Tabata et al., 2009, 2012, 2013; Miyoshi and Fishell, 2012; Inoue et al., 2014). To further clarify the role of Prdm16 in the regulation of multipolar cells, we analyzed NeuroD1 promoter activity and expression levels. Using IUE at E13.5 in the presence of a *NeuroD1* promoter-driven mCherry reporter plasmid (Miyoshi and Fishell, 2012), we tested the role of Prdm16 expression in NeuroD1-positive multipolar cells *in vivo*. These experiments showed that Prdm16 gain of function increases and expands numbers of *NeuroD1*-positive cells with multipolar morphology (Fig. 5A, bidirectional arrow; Fig. S3D), and some multipolar cells were present even in the VZ of Prdm16 gain of function (Fig. 5A, arrows). However, Prdm16 loss of function decreased numbers of *NeuroD1*-positive cells, and whereas *NeuroD1* promoter activity was significantly increased in Prdm16 overexpressing cells, it was significantly decreased in Prdm16 knockdown primary cultures (Fig. 5B). A similar phenotype was reproduced by the introduction of another knockdown vector, sh2-Prdm16, indicating that the effect of Prdm16 knockdown is not non-specific (Fig. S4A). In addition, we performed IUE in E14.5 *NeuroD1p*-EGFP reporter mouse line and confirmed that Prdm16 gain of function increases in EGFP-positive cells and in some EGFP-positive cells, even in the VZ (Fig. 5C, arrows), as shown in Fig. 5A. Another characteristic defect of Prdm16 knockdown cells was the increased *in vitro* and *in vivo* expression of Unc5D and Prdm8 (Fig. S4C,D), which is a marker of the terminal multipolar phase (Inoue et al., 2014). This finding suggests that the upregulation of Prdm16 expands *NeuroD1*-positive early multipolar phase cells, whereas downregulation causes these cells to skip the early multipolar phase (*NeuroD1*-positive multipolar cells) and prematurely transfer into late (Unc5D-positive multipolar cells) or terminal (Prdm8-positive multipolar cells) multipolar phases (Miyoshi and Fishell, 2012; Inoue et al., 2014).

Prdm16 contains seven repeats of the C_2H_2 zinc-finger domain at its N terminus (ZF1) and three similar repeats at its C terminus (ZF2), and has been shown to bind specific DNA sequences directly through two sets of zinc fingers (Nishikata et al., 2003). To determine whether the effects of Prdm16 overexpression depend on its DNA-binding properties, we constructed CAG promoter-driven mutant plasmids lacking PR (ΔPR), ZF1 (ΔnZF) and ZF2 domains (ΔcZF; Fig. S4E), and compared the resulting functions with those of an expression vector encoding full-length Prdm16. In these experiments, pCAG-Prdm16ΔPR and ΔcZF, but not ΔnZF, significantly induced NeuroD1 promoter activity in Neuro2a cells (Fig. 5D). Subsequently, we examined sh-Prdm16 using IUE with Prdm16 expression plasmids to determine whether migration defects could be rescued (Fig. S4F). IUE of full-length Prdm16, ΔPR or ΔcZF, but not ΔnZF, in the presence of sh-Prdm16 plasmid expression led to partial rescue of migration defects, suggesting that Prdm16 mediates induction of NeuroD1-positive multipolar cells and that Prdm16 function depends on the nZF domain, which is typically found in neocortical cells.

NeuroD1 represses Prdm16 expression in multipolar cells

Overexpression of NeuroD1 in dissociated cortical cells dramatically suppressed Prdm16 expression (Fig. 5E). Taken with immunostaining patterns (Fig. 3B′″,C″,G), these data indicate that Prdm16 expression was restricted to VZ (strongly) and MAZ (weakly) cells. In addition, following initial expression of Prdm16 in progenitors, NeuroD1 expression was induced in MAZ cells (Fig. 3C″) and Prdm16 expression was not detected in NeuroD1-expressing multipolar cells. Moreover, Prdm16 immunostaining of NeuroD1 loss-of-function brains showed increased populations of Prdm16-expressing cells located ectopically above the VZ (Fig. S5A, arrows), indicating that Prdm16 induces the expression of NeuroD1, which then represses Prdm16.

To investigate NeuroD1 feedback regulation against Prdm16 at specific time points, we sorted cells using FACS at 24, 36 and 48 h after IUE of control or sh-NeuroD1 with GFP plasmids on E14.5, and compared Prdm16 mRNA expression levels. In control cells, Prdm16 expression levels were dramatically decreased from 24 to 48 h, whereas NeuroD1 loss-of-function cells showed maintenance of Prdm16 expression at 36 and 48 h after IUE (Fig. 5F). Taken together, these results suggest that negative-feedback regulation of Prdm16 expression by NeuroD1 plays a crucial role in the normal progression of multipolar cells.

Analysis of time-lapse images of Prdm16 gain- and loss-of-function cells

Because Prdm16 function appears to be essential for multipolar migration, we examined the role of Prdm16 in neuronal migration and morphology using live imaging. To achieve this, we performed IUE at E14.5 and examined neuronal migration and morphology after 42 h. Subsequent time-lapse imaging analyses revealed striking differences in migration profiles between control and Prdm16 gain-of-function cells (Movie 4). In control experiments, GFP-positive neurons transformed from multipolar to bipolar shapes in the upper IZ, smoothly migrated into the CP and then moved to the pial surface (Fig. 6A). By contrast, some Prdm16 gain-of-function cells transformed into multipolar cells in the VZ; they were prevented from constructing the MAZ and remained stranded in the VZ, but showed multipolar morphology and characteristic irregular migration (Fig. 6B). Average migration distances were also decreased in Prdm16 gain-of-function cells (P<0.0001) owing to abnormal morphological changes and polarity (Fig. 6C).

Development (2017) 144, 385-399 doi:10.1242/dev.136382

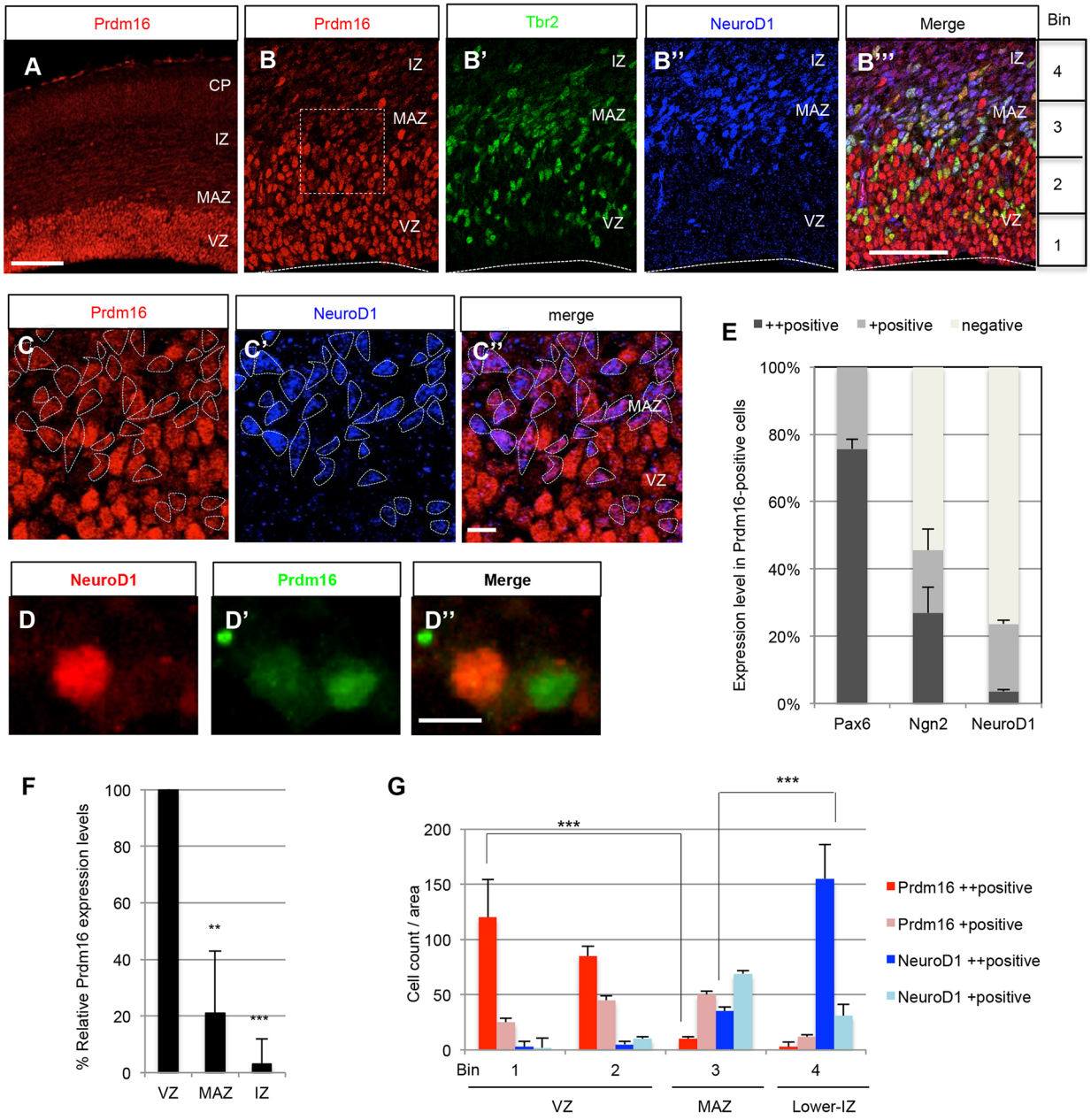

Fig. 3. The candidate mtROS regulator Prdm16 is predominantly expressed in neural progenitor cells and is markedly downregulated in postmitotic NeuroD1-positive cells. (A) Immunostaining revealed that Prdm16 was highly expressed in the VZ. Scale bars: 300 µm. (B-B‴) Prdm16-positive cells at E14.5 did not overlap with NeuroD1-positive cells (red, Prdm16; blue, NeuroD1; green, Tbr2). Scale bar: 100 µm. (C-C″) High-power images showing complementary expression between Prdm16 and NeuroD1. Scale bar: 10 µm. (D-D″) Primary dissociated E14.5 neocortical cells were cultured for 1 day. Consistent with immunostaining data, shifts of Prdm16 expression from ON to OFF matched those of NeuroD1 expression from OFF to ON. Scale bar: 10 µm. (E) Percentages of cells strongly (++) and weakly (+) positive or negative for Pax6, Ngn2 and NeuroD1 in Prdm16-positive primary neocortical cells. More than 200 cells were counted from three independent experiments. (F) To distinguish the MAZ (GFP-positive area; Fig. S2C), the VZ (GFP-negative area below the MAZ) and the IZ (GFP-negative area above the MAZ), IUE of CAG-EGFP plasmids was performed at E14.5 and immunohistochemical expression of Prdm16 was analyzed at 36 h. $^{**}P<0.001$, $^{***}P<0.0001$. (G) The developing cortex from the ventricle surface to the lower region of the IZ at E14.5 (Fig. 3B‴) was divided into four bins, and numbers of cells strongly (++) or weakly (+) positive for Prdm16 or NeuroD1 were quantified in independent sections (n=5) from five individual brains. $^{***}P<0.0001$.

In further studies, time-lapse imaging experiments were performed at a different time point (E13.5) to investigate morphological impairments of the same stages as in Fig. 5A in Prdm16 gain- and loss-of-function cells (Fig. 6D; Movie 5). Prdm16 gain-of-function cells possessed multipolar morphologies even in the VZ; this was consistent with the data presented in Fig. 5A,C. Moreover, both gain- and loss-of-function cells showed inhibition of CP invasion and aberrant migration profiles (Fig. 6E,F). These time-lapse images further suggest that Prdm16 is involved in the transition of progenitors into multipolar cells.

Prdm16-mediated regulation of multipolar cells plays a critical role in laminar formation

To further assess the roles of Prdm16 during neural differentiation, we examined control, gain- and loss-of-function cells at postnatal day of 5 (P5) after IUE at E12.5. In the presence

Development (2017) 144, 385-399 doi:10.1242/dev.136382

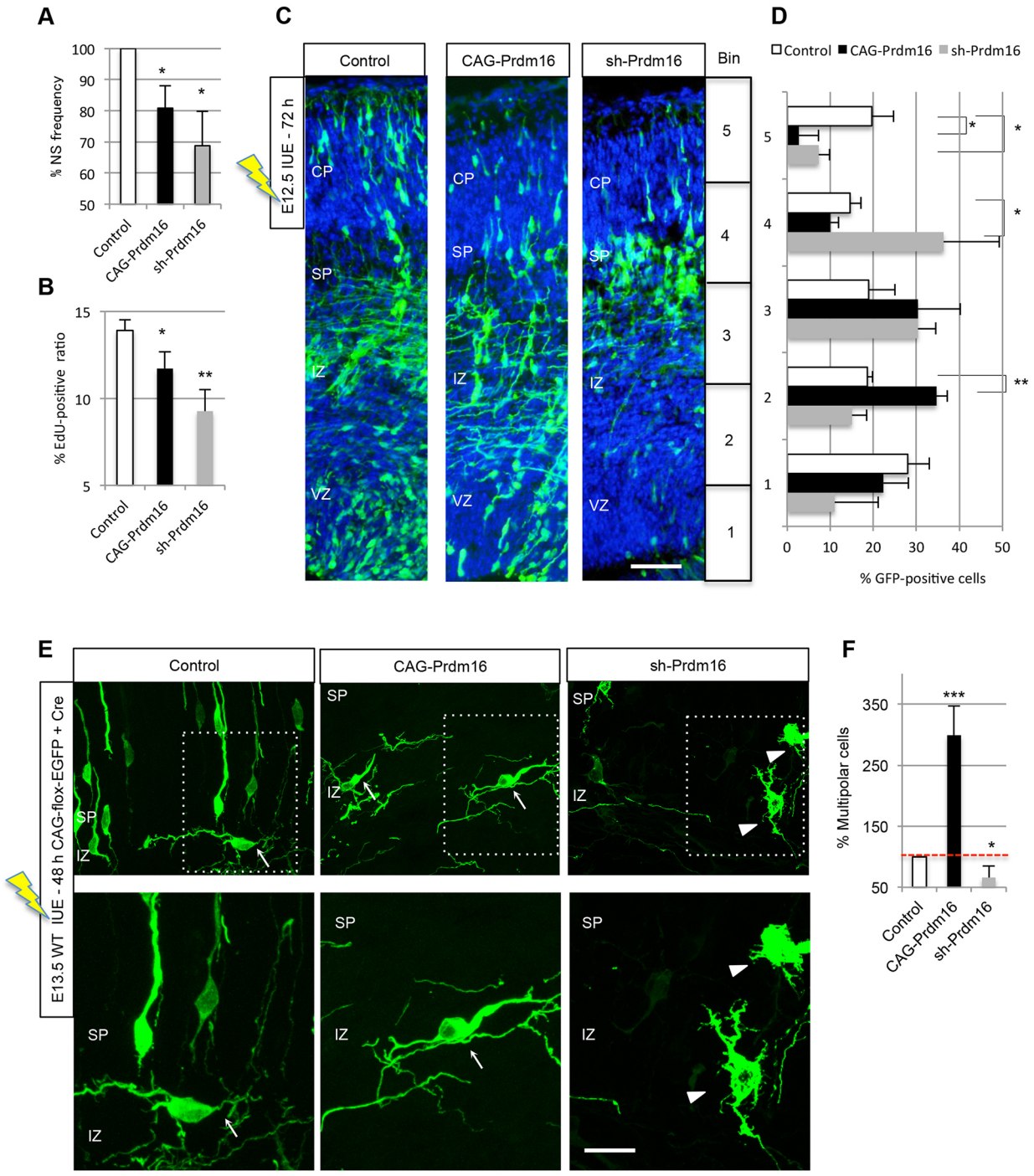

Fig. 4. Prdm16 is required for appropriate development of postmitotic multipolar cells. (A) After transfection, cells were cultured in NS media for 2 days and EGFP-positive cells were then isolated using FACS. Isolated cells were further cultured for 7 days and NS frequencies were assayed; **P*<0.01; *n*=10 independent experiments. (B) After transfection, cells were plated onto adherent substrate and EdU was added to the cultures on the next day; **P*<0.01, ***P*<0.001; *n*=5 independent experiments. (C) IUE of control, Prdm16 gain-of-function and loss-of-function vectors with pCAG-EGFP was performed at E12.5, and brains were then analyzed 72 h after electroporation. Sections are stained using DAPI (blue) to visualize nuclei. Scale bar: 100 µm. (D) The cortex was divided into five bins and the percentages of EGFP-positive cells were quantified. Eight independent experiments from different littermates were performed; **P*<0.01, ***P*<0.001; *n*=12 independent experiments from different electroporated brains. (E) Migrating cells around the SP were labeled with the Cre-loxP expression plasmids pCAG-FloxP-EGFP-N1 and pCAG-Cre in the presence of either control, pCAG-Prdm16 or psh-Prdm16 using IUE. Scale bars: 10 µm. Arrows and arrowheads indicate typical multipolar cells and aberrant cells, respectively. High-power images are shown in the lower panels. (F) Percentages of cells with multipolar morphology were noted in IUE sections; **P*<0.01, ****P*<0.0001; *n*=15 independent experiments from five individual brains.

of the control vector, GFP-positive neurons were found in layers II-VI of the neocortex at P5 (Fig. 7A). By contrast, following transfection with the Prdm16 overexpression vector (Fig. 7B,D), GFP-positive neurons did not enter the CP correctly and were primarily localized at the boundary between CP and white matter. In addition, ectopic GFP-positive neurons maintained NeuroD1 expression until postnatal stages (Fig. 7E-E″). By contrast, in the presence of a Prdm16 knockdown vector, GFP-positive neurons

Development (2017) 144, 385-399 doi:10.1242/dev.136382

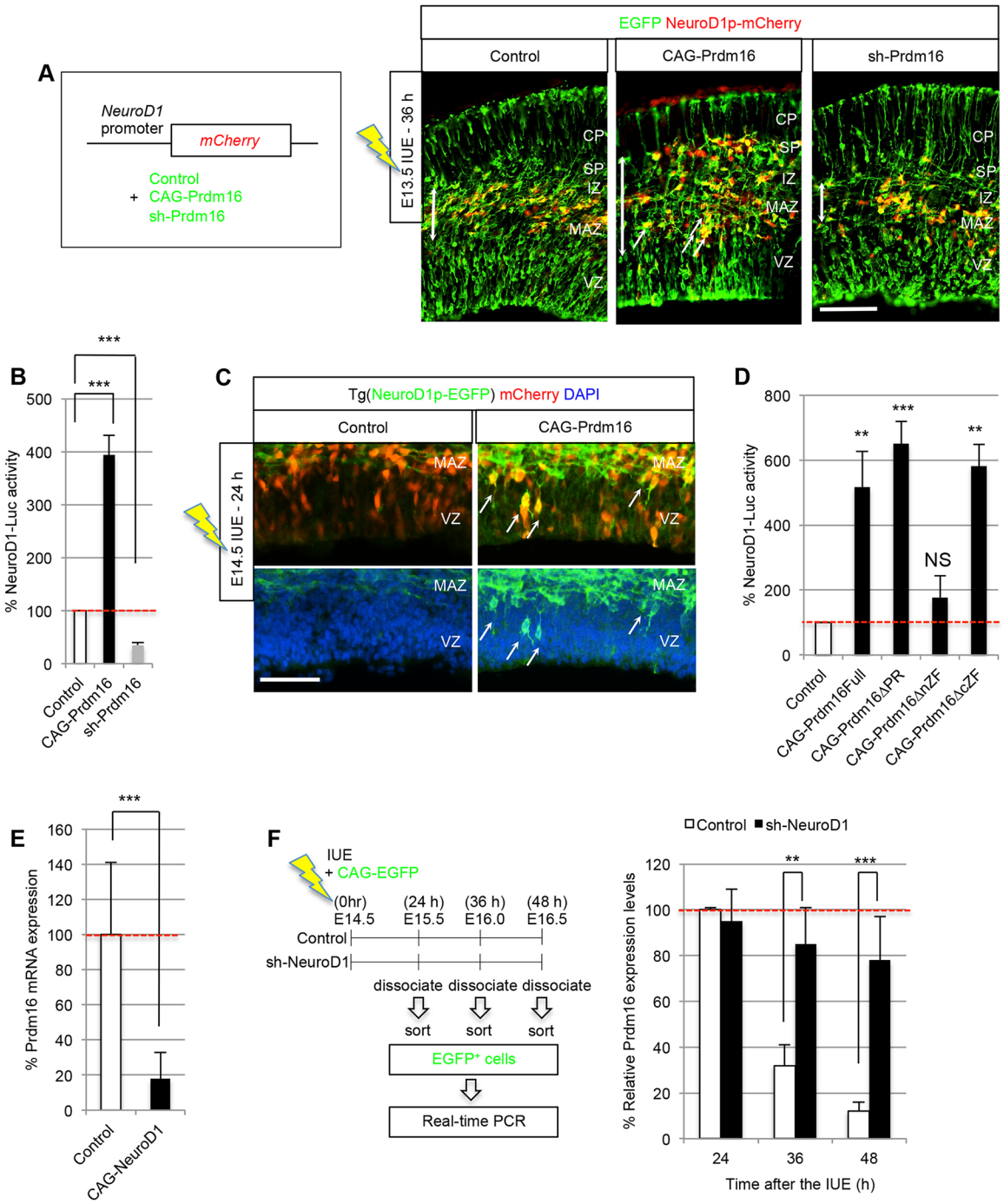

Fig. 5. Prdm16 directs normal NeuroD1 expression in multipolar cells. (A) IUE of control and Prdm16 gain- or loss-of-function vectors with pCAG-EGFP in the presence of NeuroD1 promoter-driven mCherry reporter plasmid, was performed at E13.5; brains were analyzed 36 h after electroporation. Immunostaining with GFP and mCherry; *n*=16 slices from eight individual brains. Scale bar: 100 µm. (B) Reporter constructs were designed to express firefly luciferase in response to NeuroD1 and were transfected into Neuro2a cells in the presence or absence of Prdm16 overexpression or knockdown vectors; ***P<0.0001; *n*=12 independent experiments. (C) IUE of control or Prdm16 GOF vector with pCAG-mCherry was performed in E14.5 *NeuroD1p*-EGFP reporter mice; brains were analyzed 24 h after electroporation. Immunostaining with GFP; nuclei were stained with DAPI; *n*=5 slices from five individual brains. Scale bar: 100 µm. (D) Prdm16 expression plasmids, including full length, ΔPR, ΔnZF and ΔcZF, were transfected into Neuro2a cells and NeuroD1-luciferase activity was determined; **P<0.001, ***P<0.0001; NS, not significant; *n*=8 independent experiments. (E) qPCR analysis of Prdm16 mRNA levels in primary neural progenitor cell cultures after GFP sorting of transfected 2-day-old cultures. Results were normalized to GAPDH expression; ***P<0.0001; *n*=5 independent experiments. (F) CAG-EGFP and sh-NeuroD1 were electroporated at E14.5 and GFP-positive cells were sorted using FACS; Prdm16 mRNA expression was determined at each time point (see cell sorting from electroporated brains in the supplementary Materials and Methods). **P<0.001, ***P<0.0001.

were located primarily in the deep layer (Fig. 7C,D). However, these GFP-positive cells were positioned below the Sox5-positive layer VI (Fig. 7F) and formed abnormally in another layer (indicated by an asterisk in Fig. 7C,F). Moreover, GFP-positive cells below the layer VI included neurons that expressed upper layer markers such as Brn2 (data not shown), and some of

Development (2017) 144, 385-399 doi:10.1242/dev.136382

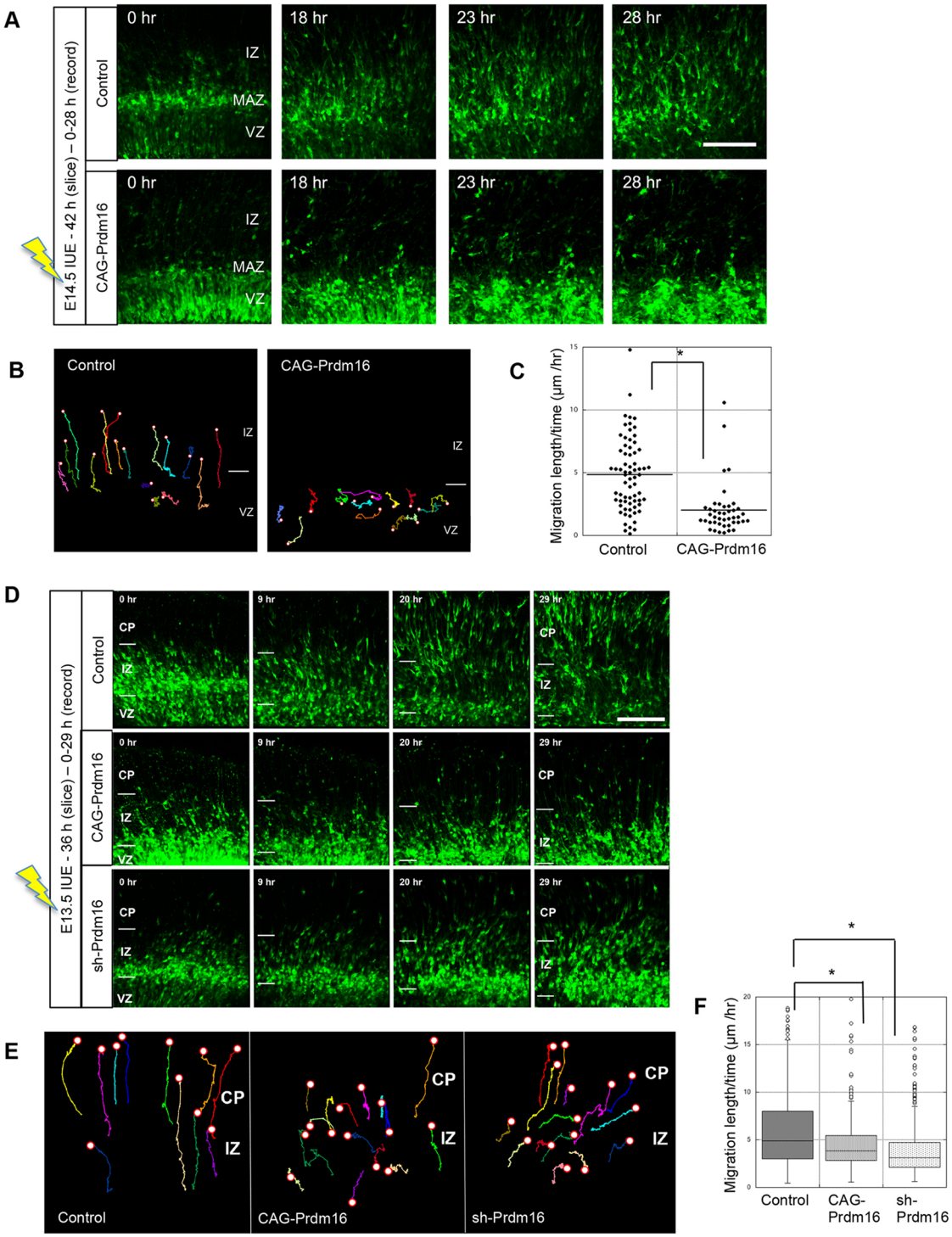

Fig. 6. Analyses of time-lapse images of Prdm16 gain-of-function and loss-of-function cells. (A-C) IUE of control or Prdm16 gain-of-function vectors was performed at E14.5. Neocortical slices were prepared about 36 h after electroporation, cultured and time-lapse images recorded. (A) Time-lapse imaging observations of Prdm16 gain-of-function cells stranded around the MAZ of electroporated cortical slices; upper panels, control cells; lower panels, Prdm16 gain-of-function cells. Scale bar: 100 µm. (B) Tracing of control (left) and Prdm16 gain-of-function (right) cells using time-lapse imaging from E16. Migratory tracks are shown as colored lines with numbers. (C) Calculation of migration speeds of control cells (left) or Prdm16 gain-of-function cells (right) with abnormal morphological changes around the MAZ. Experiments were repeated three times independently with similar results. **P*<0.01 (Student's *t*-test); more than 600 cells/group were analyzed. (D-F) IUE of control, Prdm16 gain-of-function or Prdm16 loss-of-function vectors was performed at E13.5, and neocortical slices were prepared about 36 h after electroporation. Slices were then cultured and time-lapse images were recorded. (D) Time-lapse imaging observations of Prdm16 gain-of-function cells showed multipolar morphologies even in the VZ; both gain-of-function and loss-of-function cells showed inhibition of invasion into the CP. Scale bar: 100 µm. (E) Tracing of control, Prdm16 gain-of-function or loss-of-function cells using time-lapse imaging from E15. Migratory tracks are shown as colored lines. (F) Calculation of migration speeds of control cells, and Prdm16 gain- and loss-of-function cells with abnormal morphological changes around the VZ, the MAZ and the IZ; experiments were repeated twice independently with similar results. **P*<0.01 (Tukey-Kramer test); more than 600 cells/group were analyzed.

Development (2017) 144, 385-399 doi:10.1242/dev.136382

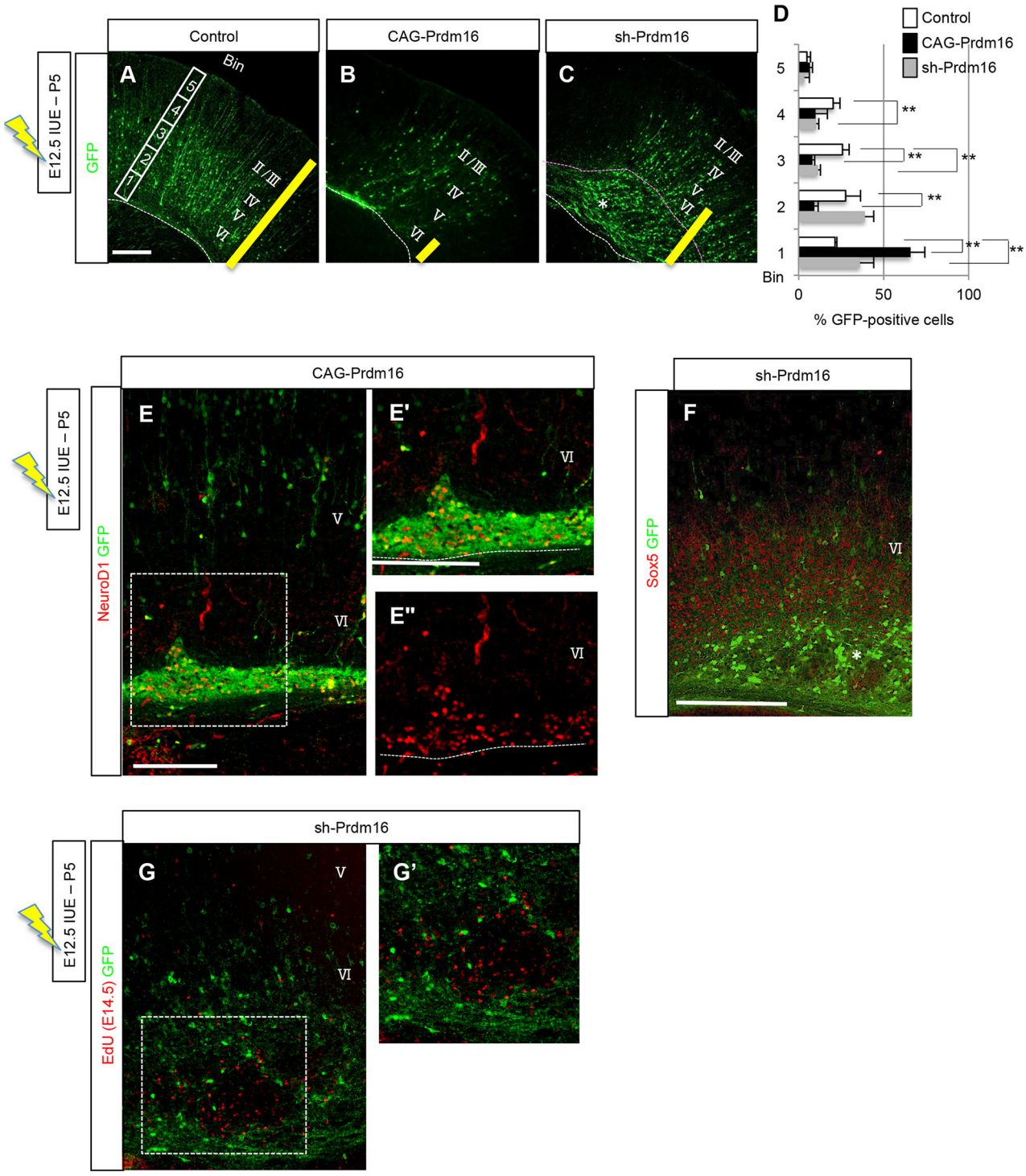

Fig. 7. Gain- and loss-of-function analysis of Prdm16 shows a marked impairment in layer formation. (A-C) IUE of control (A), and Prdm16 gain- (B) or Prdm16 loss-of-function (C) vectors at E12.5 with analysis at P5. (D) Distribution of EGFP-positive cells decreased significantly in lower bins in pCAG-Prdm16- and psh-Prdm16-electroporated brains; n=15 slices from five individual brains, $^{**}P<0.001$. (E-E″) High-power images showing that Prdm16-overexpressing cells have maintained NeuroD1 expression. Scale bars: 100 µm. (F) High-power images showing that Prdm16 knockdown cells form the aberrant layer beneath the Sox5-positive layer VI after IUE of the knockdown vector at E12.5 and analysis at P5. (G) EdU pulse labeling was performed at E14.5 after IUE of the knockdown vector at E12.5 and was analyzed at P5. Scale bar: 100 µm in F for F,G.

these cells originated from late-born cells (Fig. 7G). Taken together, these results suggest that Prdm16-mediated regulation of multipolar cells plays a crucial role in laminar formation (Fig. S6A).

Prdm16 and NeuroD1 coordinate PGC1α activation through the insulin-responsive element DNA-binding motif

We performed gene expression profiling of sorted Prdm16 gain-of-function cells from dissociated neocortical cells at E14.5 (Table 2).

Development (2017) 144, 385-399 doi:10.1242/dev.136382

Table 2. Microarray analysis of control versus Prdm16 gain-of-function cells

Gene symbol	Fold change	Gene name
Prdm16	19.11	PR domain containing 16
Ebf3	3.54	Early B-cell factor 3
Ebf2	2.45	Early B-cell factor 2
Wnt5a	2.36	Wingless-related MMTV integration site 5A
Tuba4a	2.07	Tubulin, alpha 4A
*Igf2**	1.91	Insulin-like growth factor 2
Nhlh1	1.9	Nescient helix loop helix 1
Epha6	1.72	Eph receptor A6
Slit1	1.68	Slit homolog1
*Atp13a3**	1.66	ATPase type 13A3
*Pgc1a**	1.62	PPAR, gammma coactivator 1 alpha
Vav3	1.58	Vav 3 oncogene
*Prmt8**	1.56	Protein arginine N-methyltransferase 8
*Mgst1**	1.56	Microsomal glutathione S-transferase 1
Gas6	1.51	Growth arrest specific 6
Apoe	1.5	Apolipoprotein E
Chd7	1.5	Chromodomain helicase DNA binding protein 7
Chmp2b	1.5	Chromatin modifying protein 2B
*Pdk2**	1.45	Pyruvate dehydrogenase kinase, isoenzyme2
Neurod1	1.45	Neurogenic differentiation 1

Gene expression profiles of control versus Prdm16-overexpressing cells after GFP sorting of transfected 1-day-old cultures; genes with expression levels that were more than 1.4-fold higher in Prdm16-overexpressing cells than in control cells are listed.

*Genes are associated with ROS regulation or were responsive to oxidative stress.

These experiments showed marked upregulation of *Igf2*, *Prmt8*, *Mgst1*, *Pdk2* and *PGC1α* (*Ppargc1a*), which are known regulators of mitochondrial metabolism and ROS balance (Handschin and Spiegelman, 2006; St-Pierre et al., 2006; Austin and St-Pierre, 2012) in Prdm16 gain-of-function cells, and were confirmed by qPCR in three independent samples (Fig. S6B).

Peroxisome proliferative activated receptor 1 (PGC1) transcriptional co-activators are the major regulators of several crucial aspects of energy metabolism. Specifically, PGC1α controls aspects of oxidative metabolism, such as mitochondrial biogenesis and respiration, by co-activating various nuclear receptors and factors that are not members of the nuclear receptor family. Recent studies show that PGC1α is a broad and powerful regulator of ROS metabolism (St-Pierre et al., 2006), and that Prdm16 activates brown fat cell characteristics by directly binding and activating PGC1α (Seale et al., 2007). Therefore, we performed transient transfection experiments in Neuro2a cells using a plasmid containing the PGC1α promoter region fused to a luciferase reporter gene (Fig. 8A). Subsequently, Prdm16 gain of function significantly increased PGC1α promoter activity, whereas NeuroD1 gain of function significantly suppressed it. This suppression of promoter activity was also observed with Prdm16 loss of function (data not shown), and was abolished with the PGC1αΔIRE promoter mutant (Fig. 8A). These data suggest that both Prdm16 and NeuroD1 act as transcription factors that coordinately regulate PGC1α activity through the insulin responsive element (IRE).

In further studies, we examined PGC1α gain of function using primary cultures with the sh-Prdm16 plasmid and determined whether mtROS levels could be rescued. These experiments confirmed partial rescue of mtROS levels following transfection with the PGC1α plasmid (Fig. 8C). Although, Prdm16 gain-of-function cells had slightly decreased mtROS levels, co-transfection of sh-NeuroD1 with Prdm16 gain-of-function vectors significantly increased mtROS levels (Fig. 8C) and mtDNA contents (Fig. S6C,D), suggesting Prdm16 positively regulates PGC1α activity and leads to the $mtROS^{high}$ phenotype, whereas NeuroD1 negatively regulates PGC1α activity and leads to the $mtROS^{low}$ phenotype. However, PGC1α represses NeuroD1 to prevent premature expression in progenitors (Fig. 8D). This transitional balance and timing is important for progression to the normal multipolar phase. Accordingly, transfection with the PGC1α plasmid partially rescued migration defects (Fig. 8B).

In summary, dynamic changes in mtROS levels occur during differentiation and the transition of progenitor cells into postmitotic multipolar cells. As a possible modulator of mtROS, Prdm16 is specifically expressed by these progenitors in the VZ. Hence, downregulation of Prdm16 just outside the VZ and complementary upregulation of NeuroD1 are crucial for the regulation of PGC1α-mediated changes in cellular redox environments (Fig. 8E). This event is required for the transition of progenitors into normal multipolar cells and the acquisition of proper laminar construction.

DISCUSSION

Emerging data indicate that stem cells possess metabolic characteristics that differ from those of differentiated cells (McGraw and Mittal, 2010). ROS stimulation of undifferentiated cells promotes neural stem cell self-renewal, whereas the same levels of ROS that are stimulatory to proliferative cells are toxic when present during differentiation. The present data show that embryonic neural progenitor cells have higher cellular ROS levels, as shown previously (Le Belle et al., 2011). Moreover, dynamic changes in ROS levels during neural differentiation were closely related to the transition of progenitor cells from proliferation to neuronal differentiation. In agreement, recent studies show that redox regulation is highly correlated with cell migration (Hurd et al., 2012). Therefore, the effects of ROS may be dependent on cellular differentiation states, and drastic morphological or migration behavioral changes likely occur in response to changes in ROS signaling.

In hematopoietic stem cells, Prdm16 regulates cellular ROS levels by specifically altering mtROS but not NADPH oxidase-generated ROS (Chuikov et al., 2010). In the developing neocortex, we found that Prdm16 expression was restricted in progenitors and was transiently downregulated in postmitotic multipolar cells of the MAZ or in the lower region of the IZ. As a transcription factor, Ngn2 plays important roles in the specification of glutamatergic neuronal differentiation, in the regulation of neuronal migration and in the activation of the downstream effector gene *Neurod1* in postmitotic cells. In the present experiments, NeuroD1 was exclusively expressed during the multipolar phase, and this expression was initiated when Prdm16 expression was downregulated. We also demonstrated that upregulation of NeuroD1 at the beginning of the multipolar phase enables termination of Prdm16 expression and facilitates progression towards the multipolar phase. Cells that overexpressed Prdm16 had elevated NeuroD1 expression, even in the VZ, and aberrant maintenance of NeuroD1 expression until the postnatal stage. They subsequently stopped migrating to the boundary between CP and white matter. Consistent with recent findings, this layer did not form properly, suggesting that the timing and duration of the multipolar phase is essential for neocortical formation (LoTurco and Bai, 2006; Yamagishi et al., 2011; Miyoshi and Fishell, 2012; Ohtaka-Maruyama et al., 2013; Inoue et al., 2014).

Translational control of mitochondrial activity and energy production is essential for normal development. A recent study demonstrated that knockout mice lacking cytoplasmic

Development (2017) 144, 385-399 doi:10.1242/dev.136382

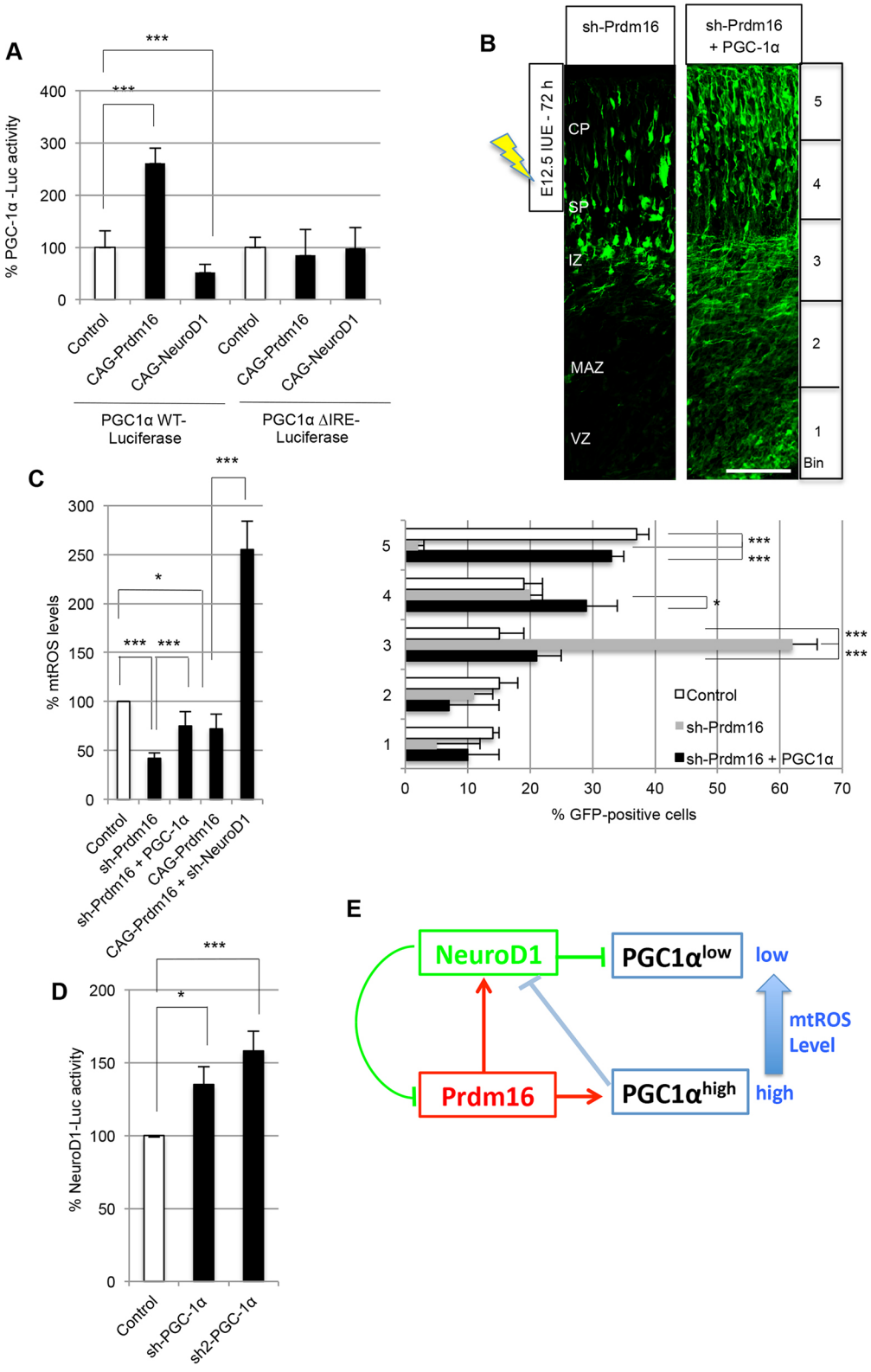

Fig. 8. Both Prdm16 and NeuroD1 regulate PGC1α activity. (A) Reporter constructs designed to express firefly luciferase in response to PGC1α or PGC1αΔIRE were transfected into Neuro2a cells in the presence or absence of Prdm16 or NeuroD1 overexpression; ***P<0.0001; n=9 independent experiments. (B) IUE of the sh-Prdm16 plasmid with the PGC1α expression plasmid at E12.5 were analyzed 72 h later. Scale bar: 100 µm. The cortex was divided into five bins, and the percentage of EGFP-positive cells was quantified; *P<0.01, ***P<0.0001; n=12 independent sections. (C) Quantitative analysis of endogenous mtROS levels in each condition in primary neural progenitor cultures from E14.5 neocortex; *P<0.01, ***P<0.0001; n=7 independent experiments. (D) Reporter constructs were designed to express firefly luciferase in response to NeuroD1 and were transfected into neocortical progenitors in the presence or absence of PGC1α knockdown vectors; *P<0.01, ***P<0.0001; n=5 independent experiments. (E) Schematic illustration of the function of Prdm16 during neocortical development. Both Prdm16 and NeuroD1 positively and negatively regulate PGC1α activity and correlate with dynamic changes in mtROS during transition of progenitors into postmitotic multipolar cells. In normal progenitors, Prdm16 activates NeuroD1 and NeuroD1 represses Prdm16. This negative-feedback regulation is important for proper morphological transition. However, PGC1α represses NeuroD1 to prevent premature expression in progenitors.

polyadenylation element-binding protein 1 have brain-specific dysfunctional mitochondria and reduced ATP levels due to defective translation of NADH dehydrogenase ubiquinone flavoprotein 2 (NDUFV2) mRNA (Oruganty-Das et al., 2012). Moreover *in utero* suppression of NDUFV2 reportedly arrested neuronal migration and impaired the multipolar-bipolar transition, suggesting that the regulation of mitochondrial function and metabolic state is crucial for multipolar migration (Chen et al., 2015).

Numerous transcription networks contribute to the regulation of cellular and mitochondrial metabolism; the PGC1 family of transcriptional co-activators have recently emerged as central regulators of metabolism (Austin and St-Pierre, 2012) and

Development (2017) 144, 385-399 doi:10.1242/dev.136382

positive regulators of mitochondrial biogenesis, gluconeogenesis and various other metabolic processes (Handschin and Spiegelman, 2006). Therefore, PGC1α-mediated control of global oxidative metabolism is an emerging concept. Accordingly, lowered oxidative metabolism was associated with decreased PGC1α activity in Prdm16 knockdown cells, and may be accompanied by decreased mtROS levels. PGC1α and Prdm16 are transcriptional co-activators that are involved in the control of energy metabolism, and their ectopic expression in white adipose tissue induces the acquisition of brown adipose tissue features (Hondares et al., 2011; Ohno et al., 2012; Ringholm et al., 2013). A recent study suggested that Sirt1 deacetylates PPARγ during energy deprivation and deacetylated PPARγ then interacts with Prdm16 to alter the balance from energy storage to energy expenditure (Qiang et al., 2012). Moreover, overexpression of PGC1α suppresses NeuroD1 mRNA expression in isolated rat and human islets (Kim et al., 2016). Similarly, we found that deletion of IRE abolished the regulation of PGC1α by Prdm16, suggesting that Prdm16 directly binds the PGC1α promoter region. We also demonstrated that PGC1α is positively or negatively regulated by both Prdm16 and NeuroD1, leading to altered mtROS levels. Furthermore, we found that PGC1α overexpression partially rescues mtROS levels in Prdm16 knockdown cells. Finally, the mtROS inhibitor and the PGC1α loss-of-function plasmid suppressed NeuroD1 activity, thus preventing premature expression of NeuroD1 in progenitors. Thus, we suggest that the transition from progenitors to multipolar cells involves dynamic changes in the cellular energy demands of the underlying mtROS environment, depending on changes in expression from Prdm16 to NeuroD1.

To our knowledge, the present data are the first to correlate mtROS regulation with neural differentiation during neocortical development. Our principal finding is that appropriate neural differentiation is highly correlated with changes in mtROS levels, which are partially regulated by the sequential expression of Prdm16 and NeuroD1. Our results suggest an important role of dynamic changes in the cellular redox environment during neural differentiation, which is essential for the proper assembly of the neocortex.

MATERIALS AND METHODS

Mice

In vivo experiments were performed in strict accordance with the recommendations in the Guide for the Care and Use of Laboratory Animals of the Doshisha University, Japan. The protocol was approved by the Committee on the Ethics of Animal Experiments of the Doshisha University. ICR mice were obtained from Shimizu Laboratory Supplies (Kyoto, Japan) and Tg(NeuroD1::GFP) bacterial artificial chromosome (BAC) transgenic mice were obtained from the GENESAT project at the Rockefeller University (NY, USA).

Plasmid construction

Prdm16 shRNA plasmid (psh-Prdm16, supplementary Materials and Methods) was kindly provided by Dr S. Kajimura (UCSF) (Ohno et al., 2012). Full-length Prdm16 cDNA clones were purchased from Addgene (catalogue number 15503). For the generation of expression plasmids, amplified Prdm16 cDNA (pCAG-Prdm16) and deletion mutants of Prdm16 (pCAG-Prdm16ΔPR, ΔcZF and ΔnZF) were inserted into pCAG-FLAG-IRES. The shRNA plasmids were generated by inserting annealed oligonucleotides into pSuper.retro.Puro vector, as previously described (Inoue et al., 2014). Target sequences were as follows: 5′-GCGAGGGC-AAGAACCATTACA-3′ for psh2-Prdm16, 5′-GCTGCTTGACTATCAC-ATACA-3′ for psh-NeuroD1, 5′-GTCAAACAAATGGTGGTTTGT-3′ for psh2-NeuroD1, 5′-GCGACCAATCGGAAATCATAT-3′ for psh2-PGC1α, and 5′-GCAATAAAGCGAAGAGCATTT-3′ for psh2-PGC1α.

In utero electroporation

Pregnant dams among wild-type ICR mice were anesthetized by intraperitoneal injection with pentobarbital. Two microliters of a mixture of plasmid DNA, which includes 2.5 mg/ml target plasmid and 0.8 mg/ml reporter plasmid, and 2 mg/ml Fast Green were directly injected into the lateral ventricles of the embryonic forebrain using a glass micropipette. Electroporation was performed using an electroporator (CUY21E, Nepa Gene) as previously described (Mizutani and Saito, 2005; Mizutani et al., 2007; Inoue et al., 2014, 2015; Yamanishi et al., 2015). The following plasmids were used in this study: pCAG-EGFP, pCAG-mCherry, pCAG-Prdm16, psh-Prdm16, psh2-Prdm16, pNeuoD1p-mCherry, psh-NeuroD1, pCAG-PGC1α, pCAG-FloxP-EGFP-N1 and pCAG-Cre.

Immunohistochemistry

Embryos were dissected, and the brains were fixed in 4% paraformaldehyde (PFA) for 1-3.5 h. For the postnatal stage, brains were fixed in 4% PFA overnight. Following 30% sucrose replacement, fixed brains were embedded in OCT compound (Sakura Tissue-Tek). The antibodies used are listed in Table S1. Immunostained sections were imaged on Zeiss LSM 710 or Olympus IX81. For details, see supplementary Materials and Methods.

Microscopy and imaging analysis

Images were acquired on a confocal microscope (LSM 710, Zeiss) or a fluorescent microscope (IX81, Olympus). ZEN and Metamorph softwares were used to acquire all confocal and fluorescent microscope images, respectively. Images were finally processed using Adobe Photoshop. 3D image processing and analysis were performed with Imaris (Bitplane). For quantification of multipolar cells around MAZ and IZ, we used a combination of molecular markers and cellular morphology. In our previous studies (Tabata and Nakajima, 2003; Tabata et al., 2009, 2012, 2013), we found that multipolar cells in the MAZ/IZ frequently had a long ascending process and a retraction bulb, representing STL morphology. These cells tended to be tangentially aligned and assumed typical multipolar cell morphology with tangentially oriented thin multiple processes. For details, see supplementary Materials and Methods.

Quantitative real-time PCR (qPCR)

qPCR was performed using SYBR Green labeling (SYBR Premix Ex TaqII, Takara) and a TP850 Real-Time PCR System (Takara). For details, see Table S2 and supplementary Materials and Methods.

DNA microarray analysis

Procedures were performed as previously described (Inoue et al., 2014). For details, see supplementary Materials and Methods.

Cell culture, *in vitro* electroporation, and mtROS quantification

Embryonic neocortical cells were isolated from E14.5 wild-type mice, followed by TrypLE Express (Gibco) treatment and trituration to generate a single-cell suspension. Plasmid DNA was introduced into primary neocortical cells using Neon Transfection System (Life Technologies). Next, neocortical neurospheres were cultured in serum-free media containing B27 without vitamin A (Gibco), N2 supplement (Gibco) and 10 ng/ml basic FGF, as previously described (Mizutani et al., 2007). Neuro2a cells were maintained in Dulbecco's modified Eagle's medium supplemented with 10% fetal bovine serum, 1% non-essential amino acids, 100 U/ml penicillin and 10 µg/ml streptomycin (Wako). mtROS levels were measured by incubating 2×10^6 cells with 5 µM MitoSox (Life Technologies) for 15 min at 37°C and analyzed using FACS.

Cell sorting

FACS analysis was performed using FACSAria II and analyzed using FACSDiva 6.1 software (Becton Dickinson). The sorted cells were collected in TRIzol (Life Technology). For details, see supplementary Materials and Methods.

Luciferase assay

A luciferase reporter assay was performed using E14.5 primary neocortical culture or Neuro2a cells. For details, see supplementary Materials and Methods.

Development (2017) 144, 385-399 doi:10.1242/dev.136382

Time-lapse imaging

E13.5 or E14.5 embryos were electroporated with pSuper-Retro-Puro (control), CAF-Prdm16 or sh-Prdm16 (2.5 µg/µl) together with pCAG-EGFP (0.8 µg/µl). Organotypic coronal brain slices (250 µm) from the level of interventricular foramen were prepared 42 h after electroporation with a vibrating microtome (HM650 V; Thermo Fisher Scientific) in Hanks' balanced salt solution (Wako), placed on an insert membrane (Millipore) and cultured in Neurobasal medium (Thermo Fisher Scientific) supplemented with 10% fetal bovine serum and 2% B27 (Thermo Fisher Scientific) as described previously (Tabata and Nakajima, 2003). The dishes were then mounted in CO_2 incubator chamber (Tokai Hit, 5% CO_2, 40% O_2) fitted onto an Olympus FV1000 confocal laser microscope. The dorsolateral region of the neocortex was observed. For details, see the supplementary Materials and Methods.

Statistical analysis

Statistical analysis was performed using Microsoft Excel. Student's *t*-test as stated in the appropriate experiments was used to test the significance. $P<0.01$ was considered to be statistically significant. Error bars indicate the s.e.m.

Acknowledgements

We thank Drs Fujio Murakami, Chiaki Ohtaka-Maruyama, Shinpei Yamaguchi, Nobuyuki Nukina, Noriko Noguchi, Yoshiro Saito and Yoichi Shinkai for helpful discussions. We also thank Drs Peter S. Rabinovitch, Ryoichiro Kageyama, Takahiko Matsuda, Goichi Miyoshi, Hiromi Shimojo, Itaru Imayoshi, Akiyoshi Fukamizu, Shingo Kajimura and Takao Kuroda for plasmids, and Mika Matsumoto for excellent technical assistance.

Competing interests

The authors declare no competing or financial interests.

Author contributions

K.M. designed this study and wrote the manuscript; M.I., R.I., H.T., D.K., M.K.-S., C.W., F.M., K.N. and K.M. performed this study and analyzed data; H.I., Y.M. and T. H. generated an antibody. All authors discussed the results and commented on the manuscript.

Funding

This research was supported by Japan Science and Technology Agency, Precursory Research for Embryonic Science and Technology (PRESTO) 'Development and Function of Neural Networks' (111832), by a Grant-in-Aid for Scientific Research on Innovative Areas 'Neurovascular' from the Ministry of Education, Culture, Sports, Science, and Technology (MEXT) of Japan (25122718) and by the Takeda Science Foundation.

Data availability

Microarray data have been deposited at ArrayExpress under accession number E-MTAB-5438.

Supplementary information

Supplementary information available online at
http://dev.biologists.org/lookup/doi/10.1242/dev.136382.supplemental

References

Austin, S. and St-Pierre, J. (2012). PGC1α and mitochondrial metabolism-emerging concepts and relevance in ageing and neurodegenerative disorders. *J. Cell Sci.* **125**, 4963-4971.

Chen, T., Wu, Q., Zhang, Y. and Zhang, D. (2015). NDUFV2 regulates neuronal migration in the developing cerebral cortex through modulation of the multipolar–bipolar transition. *Brain Res.* **1625**, 102-110.

Chuikov, S., Levi, B. P., Smith, M. L. and Morrison, S. J. (2010). Prdm16 promotes stem cell maintenance in multiple tissues, partly by regulating oxidative stress. *Nat. Cell Biol.* **12**, 999-1006.

Costa, M. R. and Hedin-pereira, C. (2010). Does cell lineage in the developing cerebral cortex contribute to its columnar organization? *Front. Neuroanat.* **4**, 1-7.

Csete, M., Walikonis, J., Slawny, N., Wei, Y., Korsnes, S., Doyle, J. C. and Wold, B. (2001). Oxygen-mediated regulation of skeletal muscle satellite cell proliferation and adipogenesis in culture. *J. Cell Physiol.* **189**, 189-196.

Hamanaka, R. B. and Chandel, N. S. (2010). Mitochondrial reactive oxygen species regulate cellular signaling and dictate biological outcomes. *Trends Biochem. Sci.* **35**, 505-513.

Hamanaka, R. B., Glasauer, A., Hoover, P., Yang, S., Blatt, H., Mullen, A. R., Getsios, S., Gottardi, C. J., DeBerardinis, R. J., Lavker, R. M. et al. (2013). Mitochondrial reactive oxygen species promote epidermal differentiation and hair follicle development. *Sci. Signal.* **6**, ra8.

Handschin, C. and Spiegelman, B. M. (2006). Peroxisome proliferator-activated receptor gamma coactivator 1 coactivators, energy homeostasis, and metabolism. *Endocr. Rev.* **27**, 728-735.

Hondares, E., Rosell, M., Díaz-Delfín, J., Olmos, Y., Monsalve, M., Iglesias, R., Villarroya, F. and Giralt, M. (2011). Peroxisome proliferator-activated receptor α (PPARα) induces PPARγ coactivator 1α (PGC-1α) gene expression and contributes to thermogenic activation of brown fat: involvement of PRDM16. *J. Biol. Chem.* **286**, 43112-43122.

Hurd, T. R., DeGennaro, M. and Lehmann, R. (2012). Redox regulation of cell migration and adhesion. *Trends Cell Biol.* **22**, 107-115.

Inoue, M., Kuroda, T., Honda, A., Komabayashi-Suzuki, M., Komai, T., Shinkai, Y. and Mizutani, K. (2014). Prdm8 regulates the morphological transition at multipolar phase during neocortical development. *PLoS ONE* **9**, e86356.

Inoue, M., Iwai, R., Yamanishi, E., Yamagata, K., Komabayashi-Suzuki, M., Honda, A., Komai, T., Miyachi, H., Kitano, S., Watanabe, C. et al. (2015). Deletion of Prdm8 impairs development of upper-layer neocortical neurons. *Genes Cells* **20**, 758-770.

Kajimura, S., Seale, P. and Spiegelman, B. M. (2010). Transcriptional control of brown fat development. *Cell Metab.* **11**, 257-262.

Kim, J.-W., You, Y.-H., Ham, D.-S., Yang, H.-K. and Yoon, K.-H. (2016). The Paradoxical effects of AMPK on insulin gene expression and glucose-Induced insulin secretion. *J. Cell. Biochem.* **117**, 239-246.

Le Belle, J. E., Orozco, N. M., Paucar, A. A., Saxe, J. P., Mottahedeh, J., Pyle, A. D., Wu, H. and Kornblum, H. I. (2011). Proliferative neural stem cells have high endogenous ROS levels that regulate self-renewal and neurogenesis in a PI3K/Akt-dependant manner. *Cell Stem Cell* **8**, 59-71.

LoTurco, J. J. and Bai, J. (2006). The multipolar stage and disruptions in neuronal migration. *Trends Neurosci.* **29**, 407-413.

McGraw, T. E. and Mittal, V. (2010). Stem cells: Metabolism regulates differentiation. *Nat. Chem. Biol.* **6**, 176-177.

Miyoshi, G. and Fishell, G. (2012). Dynamic FoxG1 expression coordinates the integration of multipolar pyramidal neuron precursors into the cortical plate. *Neuron* **74**, 1045-1058.

Mizutani, K.-i. and Saito, T. (2005). Progenitors resume generating neurons after temporary inhibition of neurogenesis by Notch activation in the mammalian cerebral cortex. *Development* **132**, 1295-1304.

Mizutani, K., Yoon, K., Dang, L., Tokunaga, A. and Gaiano, N. (2007). Differential Notch signaling distinguishes neural stem cells from intermediate progenitors. *Nature* **449**, 351-356.

Moliner, A., Enfors, P., Ibáñez, C. F. and Andäng, M. (2008). Mouse embryonic stem cell-derived spheres with distinct neurogenic potentials. *Stem Cells Dev.* **17**, 233-243.

Nadarajah, B., Brunstrom, J. E., Grutzendler, J., Wong, R. O. and Pearlman, A. L. (2001). Two modes of radial migration in early development of the cerebral cortex. *Nat. Neurosci.* **4**, 143-150.

Nishikata, I., Sasaki, H., Iga, M., Tateno, Y., Imayoshi, S., Asou, N., Nakamura, T. and Morishita, K. (2003). A novel EVI1 gene family, MEL1, lacking a PR domain (MEL1S) is expressed mainly in t(1;3)(p36;q21)-positive AML and blocks G-CSF-induced myeloid differentiation. *Blood* **102**, 3323-3332.

Noctor, S. C., Martínez-Cerdeño, V., Ivic, L. and Kriegstein, A. R. (2004). Cortical neurons arise in symmetric and asymmetric division zones and migrate through specific phases. *Nat. Neurosci.* **7**, 136-144.

Ohno, H., Shinoda, K., Spiegelman, B. M. and Kajimura, S. (2012). PPARγ agonists induce a white-to-brown fat conversion through stabilization of PRDM16 protein. *Cell Metab.* **15**, 395-404.

Ohtaka-Maruyama, C., Hirai, S., Miwa, A., Heng, J. I.-T., Shitara, H., Ishii, R., Taya, C., Kawano, H., Kasai, M., Nakajima, K. et al. (2013). RP58 regulates the multipolar-bipolar transition of newborn neurons in the developing cerebral cortex. *Cell Rep.* **3**, 458-471.

Oruganty-das, A., Ng, T., Udagawa, T., Goh, E. L. K. and Richter, J. D. (2012). Article translational control of mitochondrial energy production mediates neuron morphogenesis. *Cell Metab.* **16**, 789-800.

Puente, B. N., Kimura, W., Muralidhar, S. A., Moon, J., Amatruda, J. F., Phelps, K. L., Grinsfelder, D., Rothermel, B. A., Chen, R., Garcia, J. A. et al. (2014). The oxygen-rich postnatal environment induces cardiomyocyte cell-cycle arrest through DNA damage response. *Cell* **157**, 565-579.

Piccoli, C., Ria, R., Scrima, R., Cela, O., D'Aprile, A., Boffoli, D., Falzetti, F., Tabilio, A. and Capitanio, N. (2005). Characterization of mitochondrial and extra-mitochondrial oxygen consuming reactions in human hematopoietic stem cells. *J. Biol. Chem.* **280**, 26467-26476.

Qiang, L., Wang, L., Kon, N., Zhao, W., Lee, S., Zhang, Y., Rosenbaum, M., Zhao, Y., Gu, W., Farmer, S. R. et al. (2012). Brown remodeling of white adipose tissue by SirT1-dependent deacetylation of Pparγ. *Cell* **150**, 620-632.

Rakic, P. (1972). Mode of cell migration to the superficial layers of fetal monkey neocortex. *J. Comp. Neurol.* **145**, 61-83.

Ringholm, S., Grunnet, K. J., Leick, L., Lundgaard, A., Munk, N. M. and Pilegaard, H. (2013). PGC-1α is required for exercise- and exercise training-induced UCP1 up-regulation in mouse white adipose tissue. *PLoS ONE* **8**, e64123.

Robinson, K. M., Janes, M. S. and Beckman, J. S. (2008). The selective detection of mitochondrial superoxide by live cell imaging. *Nat. Protoc.* **3**, 941-947.

Saretzki, G., Armstrong, L., Leake, A., Lako, M. and von Zglinicki, T. (2004). Stress defense in murine embryonic stem cells is superior to that of various differentiated murine cells. *Stem Cells* **22**, 962-971.

Schriner, S. E., Linford, N. J., Martin, G. M., Treuting, P., Ogburn, C. E., Emond, M., Coskun, P. E., Ladiges, W., Wolf, N., Van Remmen, H. et al. (2005). Extension of murine life span by overexpression of catalase targeted to mitochondria. *Science* **308**, 1909-1911.

Seale, P., Kajimura, S., Yang, W., Chin, S., Rohas, L. M., Uldry, M., Tavernier, G., Langin, D. and Spiegelman, B. M. (2007). PGC-1α is required for exercise- and exercise training-induced UCP1 up-regulation in mouse white adipose tissue. *Cell Metab.* **6**, 38-54.

Seale, P., Bjork, B., Yang, W., Kajimura, S., Chin, S., Kuang, S., Scimè, A., Devarakonda, S., Conroe, H. M., Erdjument-Bromage, H. et al. (2008). PRDM16 controls a brown fat/skeletal muscle switch. *Nature* **454**, 961-967.

Seo, S., Lim, J.-W., Yellajoshyula, D., Chang, L. W. and Kroll, K. L. (2007). Neurogenin and NeuroD direct transcriptional targets and their regulatory enhancers. *EMBO J.* **26**, 5093-5108.

Shadel, G. S. and Horvath, T. L. (2015). Mitochondrial ROS signaling in organismal homeostasis. *Cell* **163**, 560-569.

Shitamukai, A., Konno, D. and Matsuzaki, F. (2011). Oblique radial glial divisions in the developing mouse neocortex induce self-renewing progenitors outside the germinal zone that resemble primate outer subventricular zone progenitors. *J. Neurosci.* **31**, 3683-3695.

St-Pierre, J., Drori, S., Uldry, M., Silvaggi, J. M., Rhee, J., Jager, S., Handschin, C., Zheng, K., Lin, J., Yang, W. et al. (2006). Suppression of reactive oxygen species and neurodegeneration by the PGC-1 transcriptional coactivators. *Cell* **127**, 397-408.

Tabata, H. and Nakajima, K. (2003). Multipolar migration: the third mode of radial neuronal migration in the developing cerebral cortex. *J. Neurosci.* **23**, 9996-10001.

Tabata, H., Kanatani, S. and Nakajima, K. (2009). Differences of migratory behavior between direct progeny of apical progenitors and basal progenitors in the developing cerebral cortex. *Cereb. Cortex* **19**, 2092-2105.

Tabata, H., Yoshinaga, S. and Nakajima, K. (2012). Cytoarchitecture of mouse and human subventricular zone in developing cerebral neocortex. *Exp. Brain Res.* **216**, 161-168.

Tabata, H., Hachiya, T., Nagata, K.-i., Sakakibara, Y. and Nakajima, K. (2013). Screening for candidate genes involved in the production of mouse subventricular zone proliferative cells and an estimation of their changes in evolutionary pressure during primate evolution. *Front. Neuroanat.* **7**, 24.

Torii, M., Hashimoto-torii, K., Levitt, P. and Rakic, P. (2009). Integration of neuronal clones in the radial cortical columns by EphA and ephrin-A signalling. *Nature* **461**, 524-528.

Tormos, K. V., Anso, E., Hamanaka, R. B., Eisenbart, J., Joseph, J., Kalyanaraman, B. and Chandel, N. S. (2011). Mitochondrial complex III ROS regulate adipocyte differentiation. *Cell Metab.* **14**, 537-544.

Trajkovski, M., Ahmed, K., Esau, C. C. and Stoffel, M. (2012). MyomiR-133 regulates brown fat differentiation through Prdm16. *Nat. Cell Biol.* **14**, 1330-1335.

Yamagishi, S., Hampel, F., Hata, K., del Toro, D., Schwark, M., Kvachnina, E., Bastmeyer, M., Yamashita, T., Tarabykin, V., Klein, R. et al. (2011). FLRT2 and FLRT3 act as repulsive guidance cues for Unc5-positive neurons. *EMBO J.* **30**, 2920-2933.

Yamanishi, E., Yoon, K., Alberi, L., Gaiano, N. and Mizutani, K. (2015). NF-κB signaling regulates the generation of intermediate progenitors in the developing neocortex. *Genes Cells* **20**, 706-719.

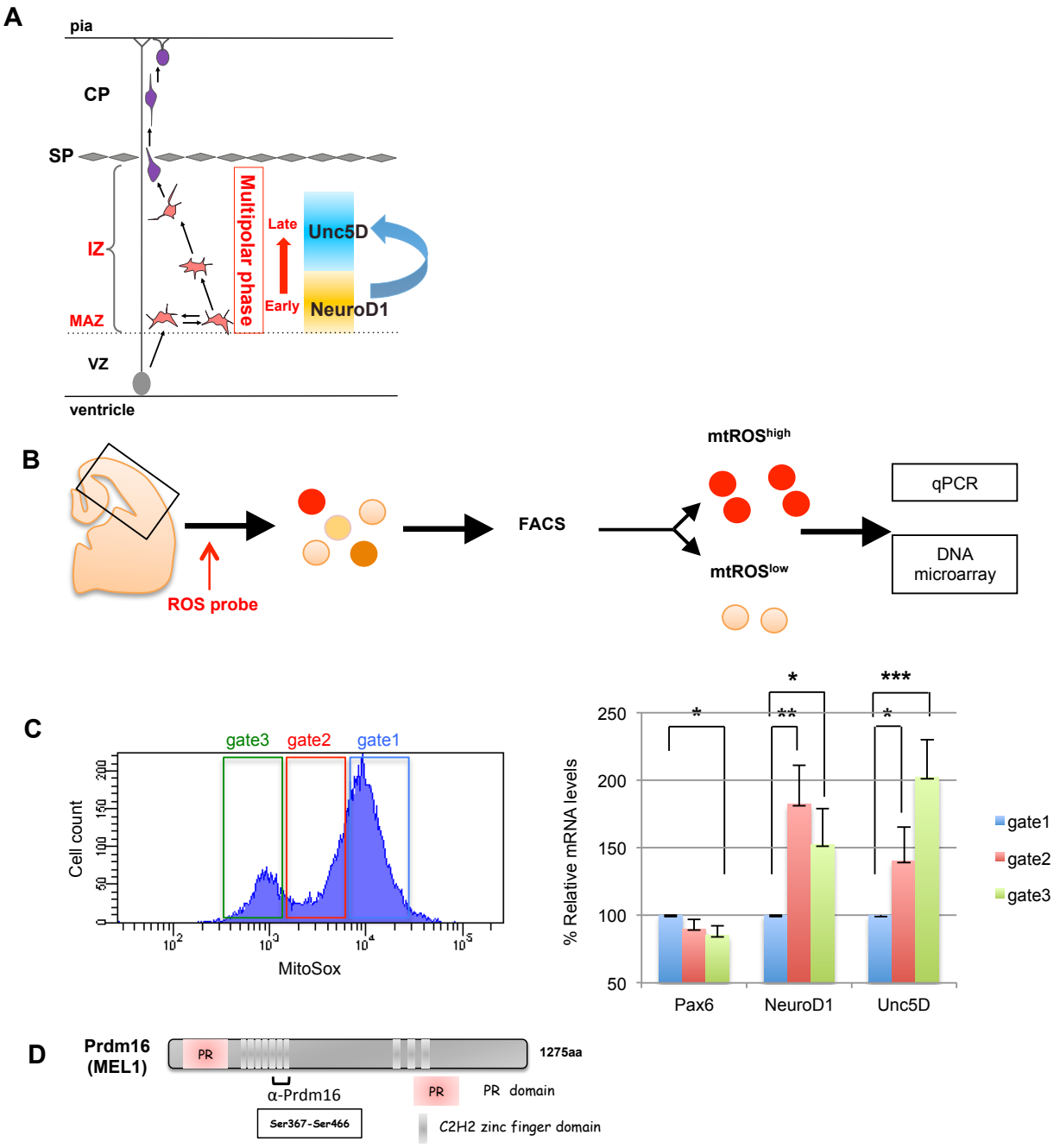

Figure S1. Progression of the postmitotic multipolar cell phase coordinates with changes in gene expression, and the changes in mtROS levels during differentiation were closely correlated with differentiation levels. (A) Schematic illustration of the sequential expression of NeuroD1 and Unc5D that coincide with early postmitotic differentiation in neocortical development (Inoue et al., 2014; Miyoshi and Fishell, 2012). (B) Schematic illustration of the experimental method for Figure 2C and D to isolate cell populations with different mtROS levels. (C) Dissociated cells were segregated into three populations according to mtROS levels and expression profiling among three sorted populations was performed using qPCR analysis. *p < 0.01, **p < 0.001, ***p < 0.0001; independent experiments from different littermates (n = 5). (D) Anti-Prdm16 antibody was generated to characterize its expression.

Development • Supplementary information

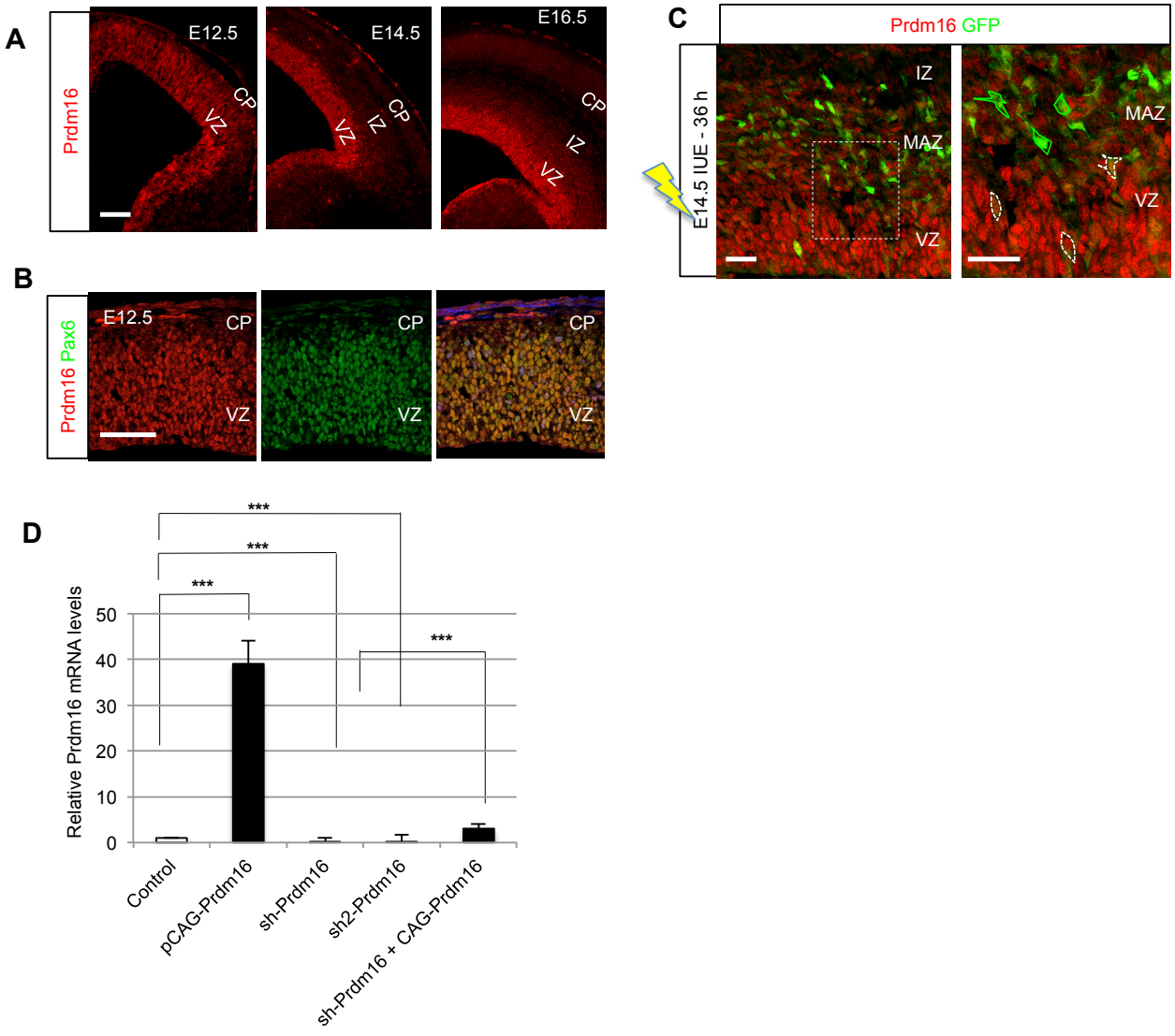

Figure S2. Prdm16 is preferentially expressed in VZ. (A and B) Immunostaining data show that Prdm16 was strongly expressed in the VZ of developing neocortex. Scale bar, 100 μm. (C) To recognize MAZ just above VZ, IUE of CAG-EGFP was introduced at E14.5 and analyzed 36 h later in accordance with a previous study (Tabata et al., 2012). Scale bar, 50 μm. (D) Both overexpression or knockdown vector for Prdm16 was transfected into primary culture, and confirmed Prdm16 mRNA levels; ***p < 0.01; independent experiments (n = 5).

Development • Supplementary information

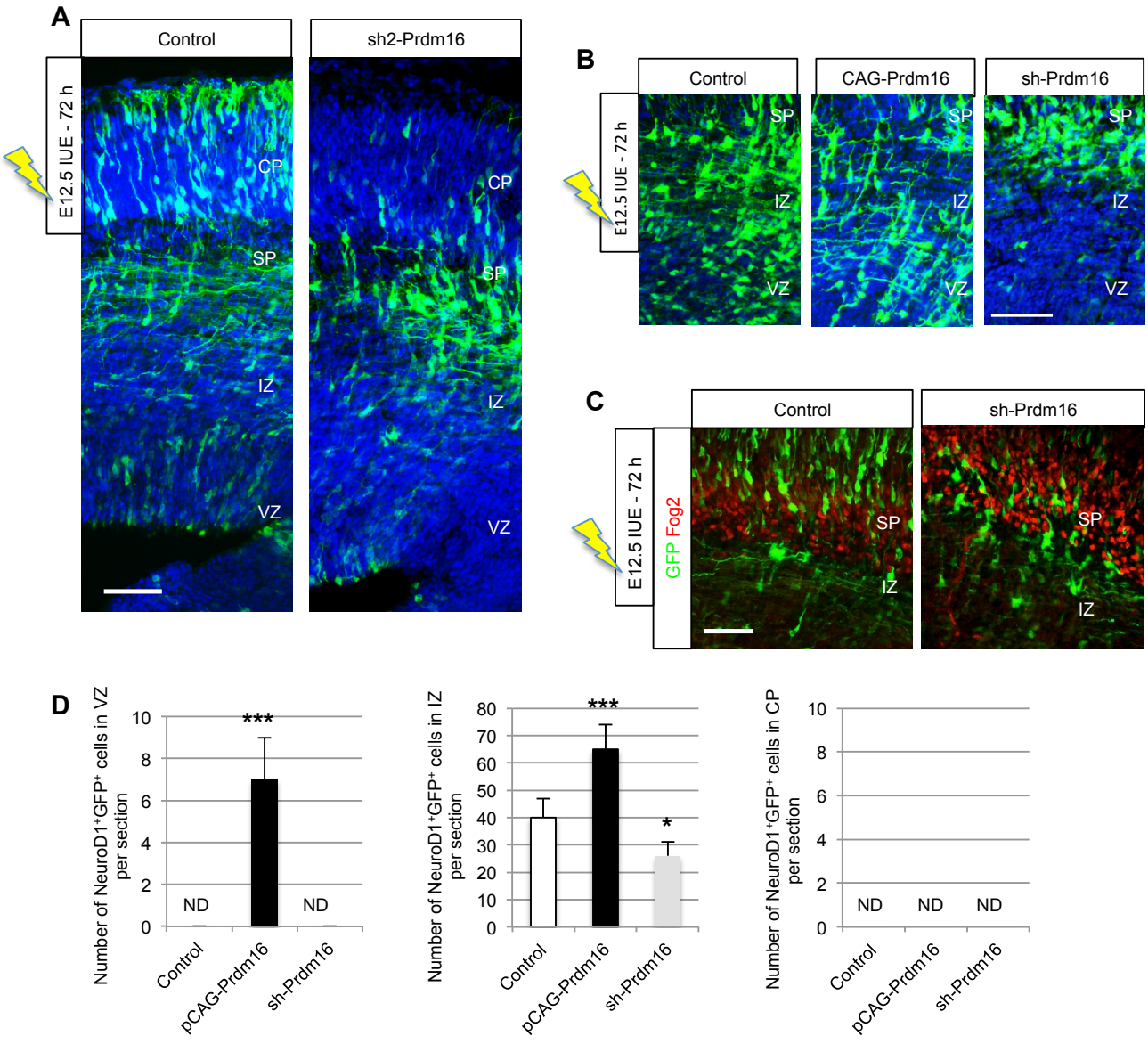

Figure S3. Prdm16 is required for appropriate development of multipolar cells.
(A) IUE of control and another Prdm16 LOF vector (sh2-Prdm16) was performed at E12.5, and brains were then analyzed 72 h after electroporation; Scale bar, 100 μm. (B) High-power images from Figure 4C; Scale bar, 100 μm. (C) Knockdown cells could not normally migrate or invade into SP, an area positive for Fog2, after IUE of the Prdm16 LOF vector at E14.5. Scale bar, 50 μm. (D) Co-IUE of sh-Prdm16 or CAG-Prdm16 in the presence of NeuroD1p-mCherry plasmids at E13.5 which were analyzed 36 h later. The cortex was divided into VZ, IZ, and CP, and the number of EGFP-positive NeuroD1-positive cells was quantified. *p < 0.01, ***p < 0.0001, ND: not detected; (n = 8 slices from eight individual brains).

Development • Supplementary information

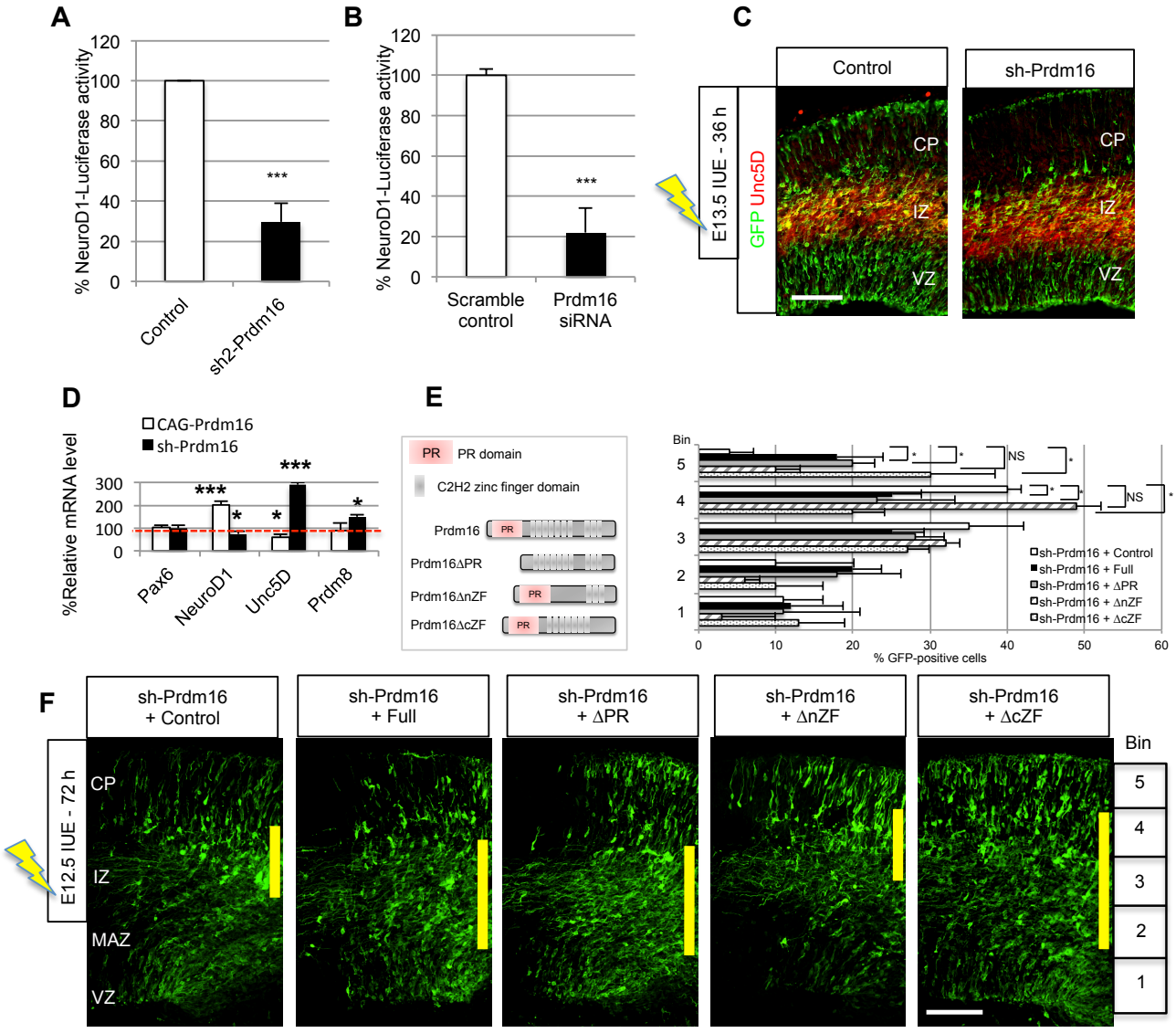

Figure S4. Prdm16 lacking nZF could not rescue migration defects induced by Prdm16 LOF.
(A and B) Reporter constructs were designed to express firefly luciferase in response to NeuroD1 and were transfected into Neuro2a cells in the presence of (A) sh2-Prdm16 or (B) Prdm16 siRNA; ***p < 0.0001; independent experiments (n = 5). (C) IUE of the control, Prdm16 GOF, or Prdm16 LOF vectors was performed at E13.5, and the brains were analyzed 36 h after electroporation. Furthermore, immunostaining with GFP and Unc5D was performed (n = 16 slices from eight individual brains). Scale bar, 100 µm. (D) qPCR analysis of marker genes in EGFP-sorted primary neural progenitor cultures after the co-transfection of CAG-EGFP and Prdm16 overexpression or knockdown vectors. *p < 0.01, ***p < 0.0001; independent experiments (n = 8). (E) Schematic illustration of a deletion mutant of Prdm16 expression vectors that lacks PR or ZF domain. (F) Co-IUE of sh-Prdm16 and CAG-Prdm16 expression plasmids or mutant plasmids ΔPR, ΔnZF, or ΔcZF at E12.5 which were analyzed 72 h later. The cortex was divided into five bins, and the proportion of EGFP-positive cells was quantified. *p < 0.01, NS: not significant; independent sections (n = 10) from five individual brains. Scale bar, 100 µm.

Development • Supplementary information

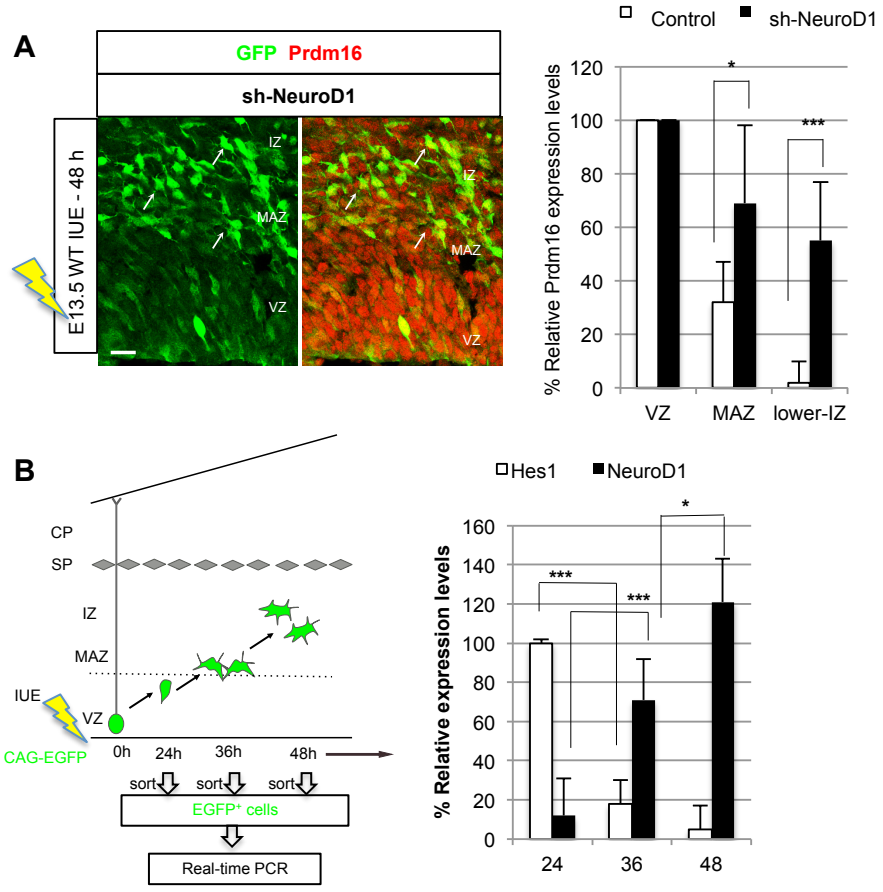

Figure S5. Prdm16 expression is negatively regulated by NeuroD1.

(A) IUE of control or NeuroD1-knockdown plasmids was performed at E13.5 and was analyzed after 48 h. Immunostaining with Prdm16 (red) was then performed to compare expression levels of Prdm16 between control and sh-NeuroD1 transfected cells. Boundaries between the VZ, the MAZ, and the IZ were deduced from orientations and densities of nuclei (Kelava 2012, Tabata 2009), and Prdm16 expression levels at each position were quantified. Cellular fluorescence intensities were analyzed using MetaMorph software and black levels were kept constant for each measurement. The pixel intensity threshold for red was adjusted so that the tissue background corresponded to level 0. About 200 randomly-selected GFP+ cells in the VZ, the MAZ, and the IZ were quantified; n = 4 slices from four individuals. Scale bar, 10 μm. *p < 0.01, ***p < 0.0001. (B) Schematic illustration of the experimental method for Figures 5F and S5B; GFP+ cell populations were isolated according to dissociation time points after IUE. Embryonic brains were harvested at 24, 36, and 48 h after the IUE of control GFP on E14.5, GFP-positive cells were sorted using FACS, and Hes1 and NeuroD1 mRNA levels were determined using qPCR. Sorted GFP+ cells were mainly from the VZ at 24 h after IUE, were mainly from the MAZ after 36 h IUE, and were mainly from the IZ after 48 h IUE, as shown previously (Tabata, 2009). To test whether NeuroD1 exerts feedback regulation against Prdm16 at specific time points (Figure 5F), GFP and sh-NeuroD1 were cotransfected with GFP plasmids on E14.5 and GFP-positive cells were sorted using FACS, and Prdm16 mRNA expression was determined (Figure 5F) at each time point. *p < 0.01, ***p < 0.0001

Development • Supplementary information

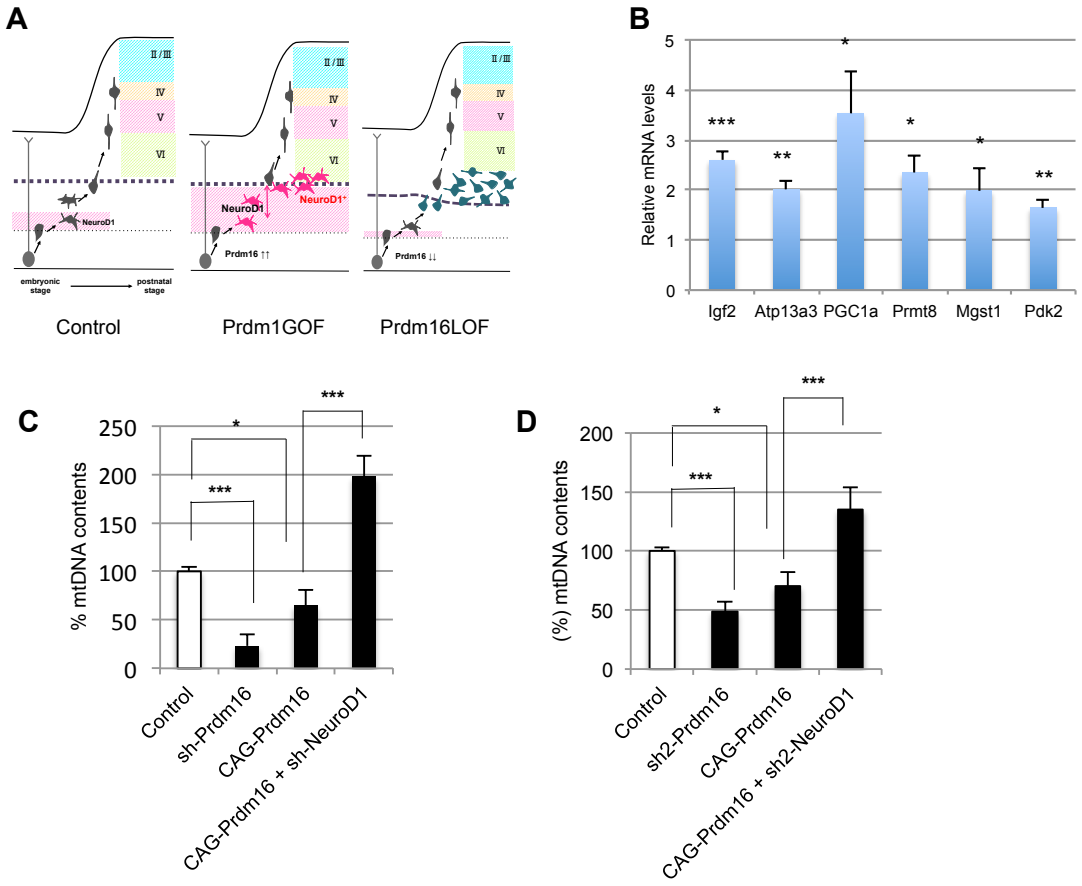

Figure S6. Co-transfection of sh-NeuroD1 with Prdm16 GOF vectors increased mtDNA contents . (A) A schematic illustration summarizes the role of Prdm16 in the control of temporal NeuroD1 expression, correlated with appropriate layer formation in the neocortex. (B) qPCR analysis of EGFP-sorted primary neural progenitor cultures after the co-transfection of CAG-EGFP and Prdm16 overexpression vectors. *p < 0.01, **p < 0.001, ***p < 0.0001; independent experiments (n = 5). (C and D) Relative mtDNA contents were determined in neocortical primary cultures transfected with (C) sh-Prdm16 or (D) sh2-Prdm16, CAG-Prdm16 in the presence or absence of (C) sh-NeuroD1 or (D) sh2-NeuroD1 ; *p < 0.01, ***p < 0.0001; independent experiments (n = 3).

Development • Supplementary information

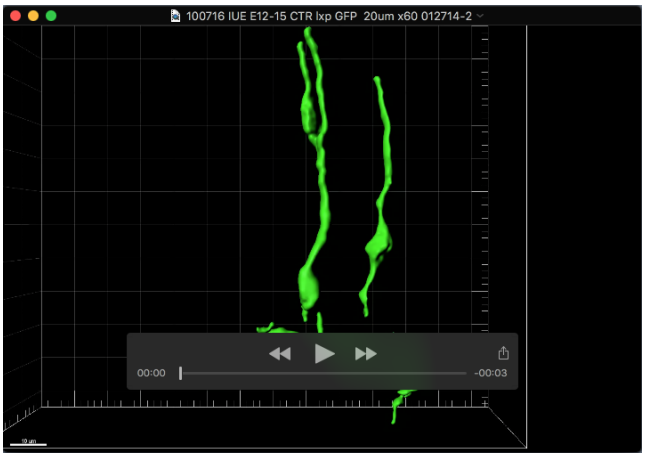

Movie 1. Clonal labeling of typical morphology of multipolar and bipolar cells in the vicinity of the SP with a Cre-loxP expression plasmid system in the presence of control plasmid. Immunofluorescence of GFP in neocortical sections at 48 h after IUE; Z-stack confocal images around the SP were reconstructed using Imaris.

Development • Supplementary information

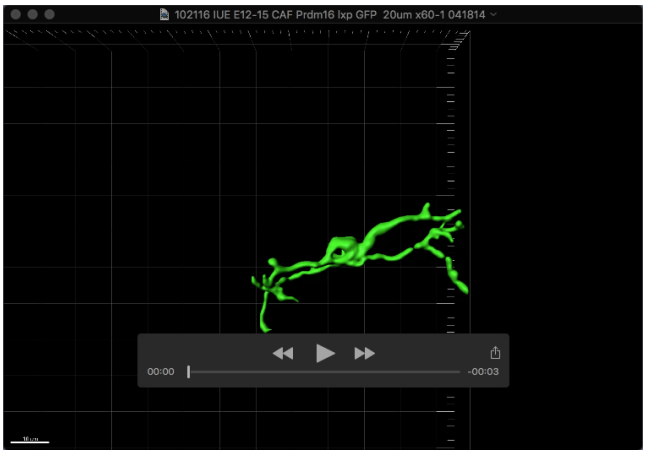

Movie 2. Clonal labeling of typical morphology of multipolar cells in the vicinity of the SP with a Cre-loxP expression plasmid system in the presence of Prdm16GOF plasmid. Immunofluorescence of GFP in neocortical sections at 48 h after IUE; Z-stack confocal images around the SP were reconstructed using Imaris.

Development • Supplementary information

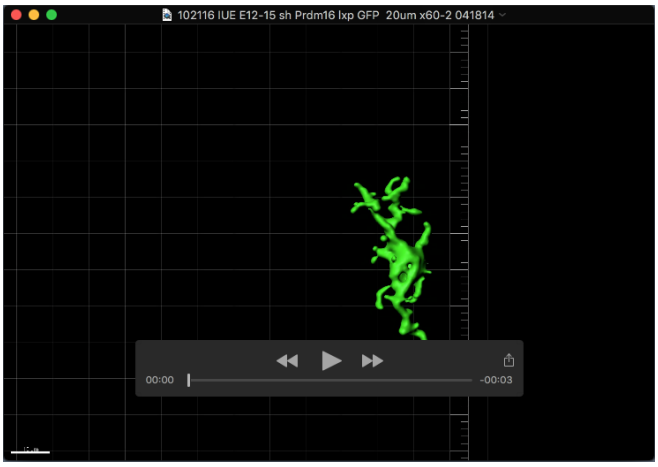

Movie 3. Clonal labeling of typical morphology of aberrant cells in the vicinity of the SP with a Cre-loxP expression plasmid system in the presence of Prdm16LOF plasmid. Immunofluorescence of GFP in neocortical sections at 48 h after IUE; Z-stack confocal images around the SP were reconstructed using Imaris.

Development • Supplementary information

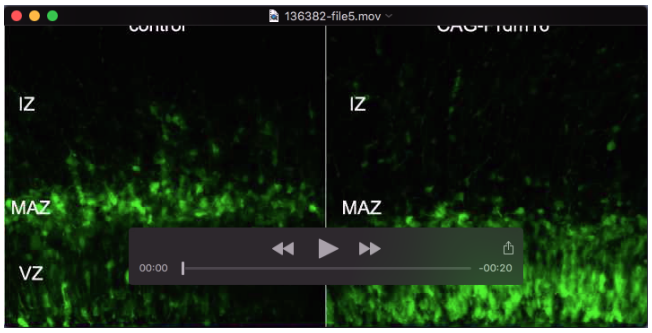

Movie 4. Prdm16-GOF cells show characteristic irregular migration in VZ, MAZ, and IZ.

IUE of control (left) or CAG-Prdm16 (right) was performed at E14.5. Cortical slices were prepared after 42 h and cultured under observation with a FV1000 confocal laser microscope. Time-lapse imaging data were then acquired automatically every 15 min for 28 h.

Development • Supplementary information

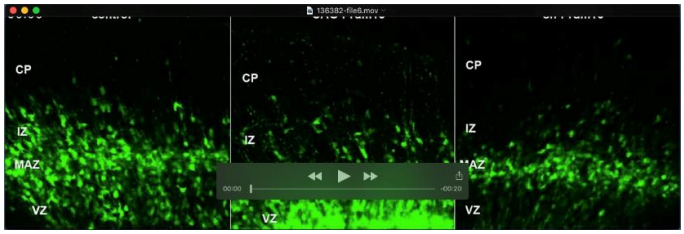

Movie 5. Prdm16-GOF cells show characteristic irregular migration, leading to the inhibition of CP invasion.

IUE of control, CAG-Prdm16 or sh-Prdm16 was performed at E13.5. Cortical slices were prepared after 36 h and cultured under observation with a FV1000 confocal laser microscope. Time-lapse imaging data were then acquired automatically every 15 min for 29 h.

SUPPLEMENTARY MATERIALS AND METHODS

Gain- and loss-of-function experiments

The knockdown efficiency of psh-Prdm16 and overexpression efficiency of pCAG-Prdm16 in the primary neural progenitors were confirmed by immunostaining (data not shown) and qPCR (supplementary material Fig. S2D). Rescue of the sh-Prdm16 phenotype was hampered by inappropriate Prdm16 levels for normal development. Thus, a second independent shRNA (sh2-Prdm16) was utilized to confirm the phenotype. Moreover, to confirm that knockdown effects of sh-Prdm16 and sh2-Prdm16 were specific to Prdm16 expression, we confirmed the absence of a phenotype relating to expression levels of the Prdm family transcription factor Prdm12 and Prdm5 (data not shown), and knockdown effect by psh-Prdm16 was rescued by the introduction of pCAG-Prdm16

Development • Supplementary information

(supplementary material Fig. S2D). The stealth RNAi for Prdm16 and its scrambled control (Thermo Fisher) were transfected with NeuroD1p-luciferase construct, and reproducibility of knockdown effect by sh-Prdm16 was confirmed (supplementary material Fig. S4B). The downregulation of Prdm16 expression by Prdm16-siRNA *in vivo* using IUE was also crucial for appropriate progression of the multipolar phase (data not shown).

Immunohistochemistry

Cryostat sections (20 μm) were treated with blocking buffer (10% donkey serum and 0.1% TritonX-100, pH 7.4) for 60 min at room temperature, followed by incubation with primary antibodies diluted (supplementary material Table S1) in the same buffer overnight at 4 degree. Sections were washed three times in 0.1% TritonX-100 (PBST) for 30 min and incubated 1 h at room temperature with secondary antibodies. The sections were washed three times in PBST for 30 min and incubated for 1 h at room temperature. After being washed, the sections were embedded on a cover glass with mounting medium (Prolong Gold, Invitrogen). For mouse anti-Prdm16 monoclonal antibody (Z1312) generation, cDNA fragments corresponding to the residues S367–S466 of mouse Prdm16 were subcloned into pBAC-surf1 (Merck Biosciences). The antibody specificity was confirmed by immunostaining against the Prdm16 knockout mouse brain, which was kindly provided by Dr. A. Moore (data not shown). EdU labeling *in vivo* (intraperitoneal injection of 12.5 mg/kg EdU) and staining were performed using the Click-IT EdU Imaging kit (Life Technologies) according to the manufacturer's instructions.

Development • Supplementary information

Microscopy and imaging analysis

We labeled multipolar cells with a Cre-loxP clonal expression plasmid system, pCAG-FloxP-EGFP-N1, and pCAG-Cre in the presence of a control, Prdm16 overexpression, or Prdm16 knockdown vector using IUE to more clearly monitor the morphological differences and counted the number of multipolar cells. Results are shown as mean ± SEM, and Student's t-test was used. n = 3 experiments brains coming from at least 3 different experiments. All images were acquired and quantified while blinded to the transfected plasmids.

Furthermore, we used IUE to more closely examine the multipolar cells. It has previously been reported that EGFP-positive cells that express NeuroD1 during the emergence of multipolar cells just above VZ, in an area called MAZ, are typically observed 36 h after IUE at E14.5 (Tabata et al., 2009, 2012, 2013). Therefore, we identified EGFP-positive cells after 36 h of IUE in MAZ, separated them into three groups positioned below SP (VZ, MAZ, and IZ), and compared the Prdm16 expression levels. For quantification, the intensity of fluorescent excitation of cells, gain and black levels were kept constant for each session of measurement, and fluorescent intensity in each cell was measured using Olympus IX81 powered by the MetaMorph analysis software. Mean data of approximately 200 cells in each region was calculated as Prdm16 expression levels for MAZ or IZ and expressed as percentage of VZ. n = 3 experiments brains coming from at least 3 different experiments.

Quantitative real-time PCR

Total RNA was isolated using RNeasy Mini Kit (Qiagen) according to the manufacturer's instruction. cDNA was synthesized from 1 μg of RNA using QuantiTect Retrotranscriptase reaction (Qiagen). qPCR was performed using SYBR green labeling (SYBR Premix Ex

Development • Supplementary information

TaqII, Takara) and a TP850 Real-Time PCR System (Takara). The primers used were listed in supplementary material Table S2. GAPDH expression was used to normalize the samples, and each sample was run in triplicate. mtDNA was quantified using qPCR with primers shown in supplementary material Table S2. The relative mtDNA copy number was calculated from the ratio of mtDNA copies to nuclear DNA (nucDNA) copies (Puente et al., 2014). The relative fold change was then calculated based on the ΔΔCt method.

DNA microarray analysis

Total RNA was prepared using a RNeasy Mini kit (Qiagen), and the quality was assessed with a BioPhotometer plus (Eppendorf). cDNA synthesis and cRNA-labeling reactions were performed using the 3′IVT-Express Kit according to manufacturer's instructions (Affymetrix). High-density oligonucleotide arrays for Mus musculus (Mouse Genome 430 2.0) containing 39,000 probes were performed according to the Expression Analysis Technical Manual (Affymetrix).

Cell sorting from electroporated brains

We harvested the embryonic brains at 24 h, 36 h, and 48 h after the IUE of control GFP on E14.5, sorted GFP-positive cells using FACS, and determined Hes1 and NeuroD1 mRNA level using qPCR. We confirmed that sorted GFP-positive cells at 24 h after the IUE contained mainly VZ cells, at 36 h contained mainly MAZ cells, and at 48 h contained mainly MAZ cells (Figure S5B); this was consistent with the results of a previous study (Tabata et al., 2009). Therefore, the same technique was utilized to compare mtDNA content during differentiation (Figure 1F) among VZ cells, MAZ cells, and IZ cells.

Development • Supplementary information

In addition, to test whether NeuroD1 exerts feedback regulation against Prdm16 at specific time points, GFP-positive cell populations were isolated according to dissociation time points after IUE. Schematic illustration of the experimental method was shown in Figures 5F. Embryonic brains were harvested at 24, 36, and 48 h after the IUE of control GFP on E14.5, GFP-positive cells were sorted using FACS, and Prdm16 mRNA expression was determined (Figure 5F) at each time point. n = 3 experiments brains coming from at least 3 different experiments.

Luciferase assay

Luciferase reporter assay was performed using E14.5 primary neocortical culture or Neuro2a cells. After transient transfection, cells were cultured for 24 h. Cell lysates were made using Dual-Luciferase Assay System (Promega), and luciferase activity of each lysate was measured in triplicate by a luminometer (GloMax®-Multi Detection System, Promega). Firefly luciferase activity was normalized relative to the activity of Renilla luciferase. The luciferase constructs for Hes1, Ngn2, NeuroD1, and PGC1α were kindly provided by Drs. H. Shimojo and A. Fukamizu, respectively.

Time-lapse imaging

Approximately 10-20 optical Z sections were acquired automatically every 15 min for about 30 h, and 20 focal planes (50 μm thick) were merged to visualize the entire shape of the cells. Representative migration trajectories of neurons observed in the control, GOF, and LOF experiments were traced using MTrackJ (a plugin for ImageJ software, NIH). The migration speed was calculated by dividing the migration distance achieved by each cell

Development • Supplementary information

by the duration of tracking. Statistical analyses shown in Figure 6C was performed using Student's t-test (Statcel 3, OMC Inc.). To analyze the migration speed in Figure 6F, the trajectories of migrating neurons were automatically traced by using TrackMate plugin (ImageJ software, NIH). The data of each group (control, GFP and LOF) were obtained from 4~6 brains in 2 independent experiments (> 600 cells/group), and the differences were assessed by one-way ANOVA and Tukey-Kramer post hoc test (Statcel 3, OMC Inc.).

Development • Supplementary information

Table S1. Antibodies list

Antibody	Supplier	Cat No.	Dilution
Goat anti-Brn2	Santa Cruz	sc-6029	1:100
Goat anti-NeuroD1	Santa Cruz	sc-1084	1:100
Goat anti-Unc5D	R&D systems	AF1429	1:100
Rabbit anti-DsRed	TaKaRa	632496	1:500
Rabbit anti-Fog2	Santa Cruz	sc-10755	1:50
Rabbit anti-GFP	Torrey Pines Biolabs	TP401	1:200
Rabbit anti-Sox5	GenWay	18-003-42358	1:200
Rabbit anti-Tbr2	abcam	ab23345	1:300
Rat anti-GFP	nacalai tesque	04404-26	1:500
PE mouse anti-CD133	eBioscience	12-1331-82	1:1000
Donkey secondary antibodies conjugated to Alexa fluorophores A488, A594, A647	Invitrogen		1:500

Development • Supplementary information

Table S2. Primer Sequences used in real-time PCR

Gene	Species	Forward Primer	Reverse Primer
Atp13a3	mouse	GAATGGGGGAGGAGCAGT	ATCCAATTCCAGCCACCA
GAPDH	mouse	AGCTTGTCATCAACGGGAAG	TTTGATGTTAGTGGGGTCTCG
Hes1	mouse	AAAGCCTATCATGGAGAAGAGGCG	GGAATGCCGGGAGCTATCTTTCTT
Igf2	mouse	AAAGCCATCTCCCCGTTC	ACTGGGATCCCCATTGGT
Mgst1	mouse	ACCTCAGGCAGCTCATGG	TGGCATTCTCTCCCTTGC
mtDNA	mouse	CCCATTCCACTTCTGATTACC	ATGATAGTAGAGTTGAGTAGCG
NeuroD1	mouse	CTCAGCATCAATGGCAACTTCTC	GACTCGCTCATGATGCGAATGCC
Ngn2	mouse	TAGGATGTTCGTCAAATCTGAGAC	CGCGCTGGAGGACATC
nucDNA	mouse	GTACCCACCTGTCGTCC	GTCCACGAGACCAATGACTG
Pax6	mouse	CCAGCATGCAGAACAGTCAC	CATCTGCATGGGTCTGCAG
Pdk2	mouse	AAAGACCCCGAGGACCAC	TGGTGCTGCCATCAAAGA
PGC1a	mouse	GAAAGGGCCAAACAGAGAGA	GTAAATCACACGGCGCTCTT
Prdm16	mouse	AGGGCAAGAACCATTACACG	AGAGGTGGTCGTGGGTACAG
Prmt8	mouse	TGCCAGGGACAAGTGGTT	TTGCTTTGGGTCCACGAT
Unc5D	mouse	CACCAGGGCTGACCATAAC	TCCATTCACGTAGACCACC

Development • Supplementary information